The Island Arc (2005) **14,** 69–90

Research Article

Petrogenesis and tectonic implications of Early Cretaceous high-K calc-alkaline volcanic rocks in the Laiyang Basin of the Sulu Belt, eastern China

FENG GUO,* WEIMING FAN, YUEJUN WANG AND CHAOWEN LI

Key Laboratory of Marginal Sea Geology, Guangzhou Institute of Geochemistry and South China Sea Institute of Oceanology, Chinese Academy of Sciences, Wushan, Guangzhou 510640, China (email: guofengt@263.net)

Abstract Early Cretaceous high-K calc-alkaline volcanism occurring in the Laiyang Basin north of the Sulu high-pressure to ultrahigh-pressure (HP-UHP) Metamorphic Belt, eastern China, comprises a wide spectrum of rock types, ranging from trachybasalts to trachydacites. The basaltic–andesitic rocks erupted at 107–105 Ma, spanning an SiO_2 range of 50.1–59.6% and an MgO range of 2.6–7.2%, and are characterized by large ion lithophile element (LILE; e.g. Ba and K) and light rare earth element (LREE) enrichment, high field strength element (HFSE) depletion and highly radiogenic Sr but non-radiogenic Nd isotopic compositions ($^{87}Sr/^{86}Sr(i) = 0.70750–0.70931$; $\varepsilon_{Nd}(t) = -17.9 - -15.6$). The geochemical similarities between these rocks and the earlier Sulu Belt lamprophyres suggest that both types of mafic rocks were derived from similar mantle sources with LILE and LREE enrichment. Thus, the Wulian–Qingdao–Yantai Fault that separates the two terranes at the surface should not be considered as a lithospheric boundary between the North China and Yangtze blocks. The felsic lavas erupted at 93–91 Ma, spanning an SiO_2 range of 61.6–67.0% and an MgO range of 1.1–2.6%, and show a trace element geochemistry similar to the basaltic rocks, but with higher radiogenic Sr and even lower Nd isotopic compositions ($^{87}Sr/^{86}Sr(i) = 0.70957–0.71109$; $\varepsilon_{Nd}(t) = -19.1 - -17.5$), similar to I-type granitoids in the Sulu Belt. A crustal origin was proposed to explain their compositions (which are comparable to those of experimental slab melts), the >10 Ma eruption interval and the compositional gaps in some elements (e.g. P, Ti and Sr) between them and the older basaltic–andesitic rocks. These melts were derived from predominant metaigneous protoliths containing mafic accumulative counterparts of the basaltic–andesitic and/or lamprophyric magmas. The extensive extrusion of Early Cretaceous high-K calc-alkaline rocks in the Laiyang Basin favored an extensional regime in response to the progressive attenuation of the thickened lithosphere and orogenic collapse, as reflected in the development of the basin from a foreland basin (before the end of the Jurassic period) to a fault basin (since the Early Cretaceous period).

Key words: Early Cretaceous period, eastern China, geochemistry, high-K calc-alkaline volcanism, postorogenic extension, Sulu Belt.

INTRODUCTION

High-K calc-alkaline volcanic rocks are usually distributed in orogenic belts, especially in the post-collisional or postorogenic stages, such as those in northeastern China (Fan *et al.* 2003), the Tibet Plateau (Turner *et al.* 1996; Miller *et al.* 1999), the European Hercynian Orogen (Rotturaa *et al.* 1998), the west Anatolia area of Turkey (Aldanmaz *et al.* 2000) and the western USA (Hawkesworth *et al.* 1995; Rogers *et al.* 1995). These melts generally show arc-like trace element signatures with

*Correspondence.

Received 12 May 2004; accepted for publication 08 December 2004.

variable large ion lithophile element (LILE) and light rare earth element (LREE) enrichment relative to high field strength element (HFSE) enrichment that is the result of previous enrichment caused by slab subduction (Turner *et al.* 1996; Miller *et al.* 1999; Aldanmaz *et al.* 2000; Fan *et al.* 2003). Being different from arc volcanics, where magma generation is usually attributed to the lowering of the peridotite solidus by the introduction of H_2O and other volatiles from the subducted slabs (Grove & Kinzler 1986; Davies & Stevenson 1992; Arculus 1994), these melts extruded under extensional regimes associated either with removal of the lithospheric root or more distributed attenuation of the previously thickened lithosphere. Their geochemical features can create important constraints on the effect of the crust–mantle interaction and enrichment process and lithospheric evolution beneath continental margins.

The Sulu high-pressure to ultrahigh-pressure (HP-UHP) Metamorphic Belt is widely accepted as the eastern extension of the Triassic Qinling–Dabie collisional orogen between the North China block (NCB) and Yangtze block (YB) (Li *et al.* 1993; Cong 1996; Jahn *et al.* 1996; Zheng *et al.* 2002). The preserved ultrahigh-pressure minerals (diamond inclusions and coesites) in eclogites and metapelites, and the clinopyroxene, apatite and rutile exsolutions in garnets suggest that the continental crust had been subducted to mantle depths even greater than 200 km (Xu *et al.* 1992; Li *et al.* 1993, 1999; Ye *et al.* 2000). The area has become one of the most important regions when discussing the mechanism for continental subduction and HP-UHP metamorphism, and the effect of mantle–crust interaction beneath the collisional belt. It appears that one of the present debates is focused on the boundary between different tectonic units, and four major faults (Fig. 1, F1–F4) have been considered as the boundary between the NCB and YB. A crustal detachment model was proposed by Li (1994), who considered the Hefei–Nanjing Fault (F1) as the Triassic suture in accordance with geophysical surveys. This hypothesis was further supported by the distinct geochemical features of the Cenozoic basalts and basalt-hosting granulite xenoliths from different tectonic units in eastern China (Chung 1999; Yu *et al.* 2003). Yin and Nie (1993) proposed that the Jiashan–Xiangshui Fault (F2) was the likely Triassic suture based on tectonic zoning and evolution. Structural deformation analysis of the Sulu Belt suggested that the boundary was located north of the Jiaodong terrane (F4) (Faure *et al.* 2001). However, many geologists (Enami *et al.* 1993; Ishizaka *et al.* 1994; Zhai *et al.* 2000) considered the Wulian–Qindao–Yantai Fault (F3) as the most likely candidate because terranes with distinguishable lithology, ages and metamorphic history occur on both sides of the fault. The key to the debate is to constrain the nature of the Mesozoic lithospheric mantle beneath different units, but this is hampered by the thick layer of Cenozoic sediments, with little exposure of the Mesozoic mafic rocks (e.g. the Subei–Jiaonan area). In the Jiaodong region of the Sulu Belt, the widely distributed Early Cretaceous volcanic rocks and lamprophyres provide a good opportunity for constraining the nature of the subcontinental lithospheric mantle (SCLM) around F3. Previous studies on Early Cretaceous basaltic lavas along the fault and lamprophyres in the Sulu UHP belt revealed an enriched mantle metasomatized by melts of the subducted crust of the Yangtze affinities (Fan *et al.* 2001; Yang & Zhou 2001; Zhou *et al.* 2002; Guo *et al.* 2004), while the nature of the SCLM north of the Sulu UHP belt is still unclear. In this paper, we report new K–Ar dating, major element, trace element and Sr–Nd isotope data of Early Cretaceous high-K calc-alkaline volcanic rocks in the Laiyang Basin, north of the Sulu UHP belt. Utilizing the published data of contemporaneous igneous rocks in the adjacent areas, this study will focus on: (i) the origin of the high-K calc-alkaline volcanic rocks; (ii) the nature of the Mesozoic SCLM north of the Sulu Belt in order to investigate the possibility of F3 being a lithospheric boundary; and (iii) understanding the relationship between extensive high-K calc-alkaline volcanism and the tectonic evolution of the Sulu collisional belt.

GEOLOGICAL BACKGROUNDS

The Laiyang Basin is located in the Jiaodong area, separated from the Sulu HP-UHP belt by F3 (Fig. 1) (BGMRS 1991; Enami *et al.* 1993; Ishizaka *et al.* 1994; Zhai *et al.* 2000). Sedimentary records indicate that it had been a foreland basin by the end of the Jurassic period, representative of the Laiyang Group, which is mainly composed of mudstones, shales and siltstones. In the Early Cretaceous period, it became a fault basin with strike-slip pull-apart character, represented by the Qingshan Group, which is composed mainly of volcanic sequences with sedimentary interbeds. It has been a rift basin since the Late Cretaceous

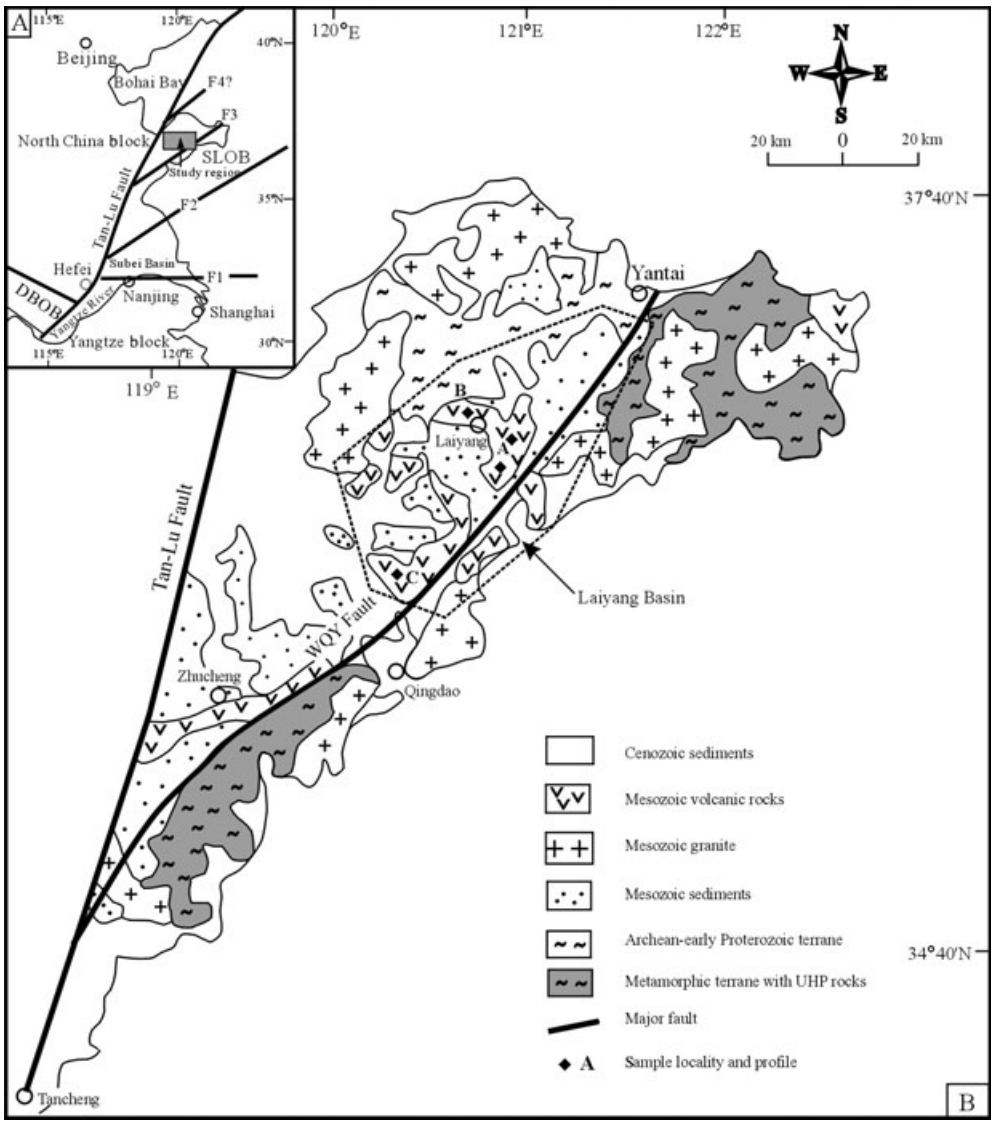

Fig. 1 A geological map of the Sulu Belt, showing the distribution of the Early Cretaceous volcanic rocks. Four faults have been considered as the lithospheric boundary between the Yangtze block and North China block: the Nanjing–Hefei Fault (F1) (Li 1994; Chung 1999; Yu *et al.* 2003), the Jiashan–Xiangshui Fault (F2) (Yin & Nie 1993), the Wulian–Qindao–Yantai (WQY) Fault (F3) (Enami *et al.* 1993; Ishizaka *et al.* 1994; Zhai *et al.* 2000) and the fault north to the Jiaodong region (F4) (Faure *et al.* 2001). DBOB, Dabie Orogenic Belt; SLOB, Sulu Orogenic Belt; UHP, ultrahigh pressure.

period, and a representative of the Wangsi Group which comprises conglomerate rocks and coarse-grained sandstones that are several kilometers thick.

Early Cretaceous volcanic rocks are widely distributed in the central and marginal parts of the basin (BGMRS 1991; Qiu *et al.* 1996; Li & He 1997). The volcanic sequences occur in horizontal or subhorizontal layers, disconformably overlying the Upper Jurassic Laiyang Group and truncating the Late Archean to Early Proterozoic metamorphic basement. At the basin center, the volcanic rocks can be divided into two groups: the predominant lower basaltic–andesitic rocks and the subordinate upper felsic lavas, separated by sedimentary interbeds that are tens to hundreds of meters thick. In the basin margins, there are also two volcanic groups, both with predominant felsic lavas. The thickness of the volcanic sequences varies from thousands to hundreds of meters, decreasing from the center to the margins of the basin.

The samples in this study were collected from two volcanic profiles at the center of the Laiyang Basin. A detailed description of the two profiles and a comparison with that in the basin margins are shown in Figure 2. The volcanic rocks comprise a wide spectrum of rock types, ranging from basalts, basaltic trachyandesites and trachyandes-

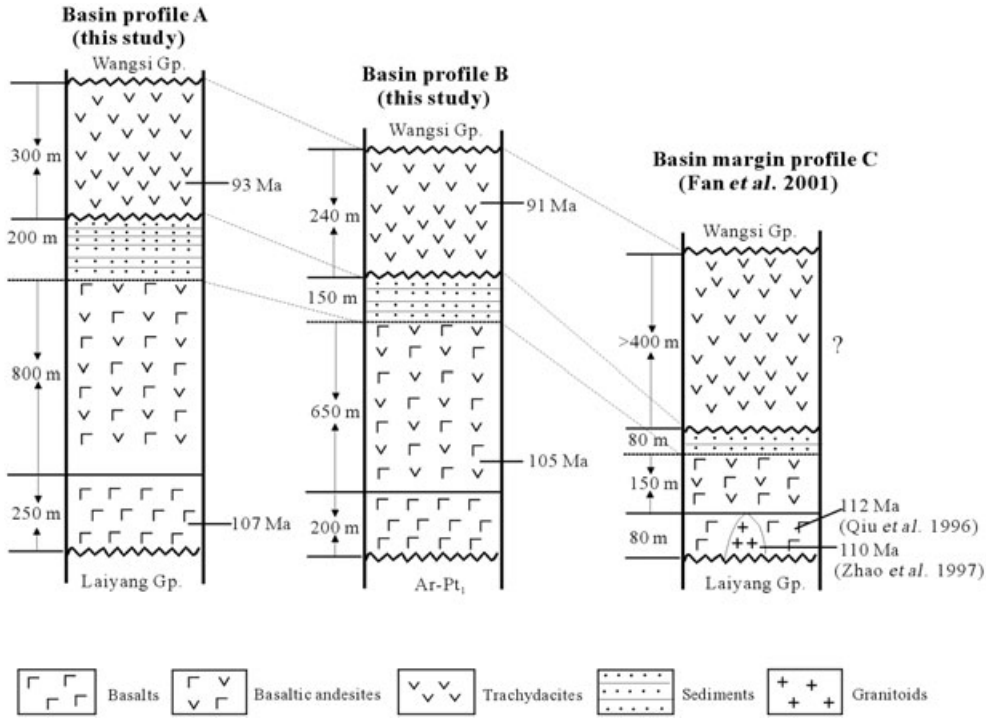

Fig. 2 Stratigraphic profiles and eruption episodes of the volcanic sequences in the Laiyang Basin. The margin profile (compiled from Fan *et al.* 2001, with permission) is presented for comparison.

ites, to trachydacites. The basaltic rocks are commonly subaphyric to weakly porphyritic, with predominant phenocrysts of clinopyroxene and plagioclase with minor olivine spanning a range of 2–4 mm in grain size. The proportions of clinopyroxene and olivine phenocrysts decrease from the basalts to basaltic trachyandesites, with an increasing proportion of plagioclase phenocrysts. The matrix is mainly composed of fine-grained clinopyroxene and plagioclase and a few opaque oxides, such as magnetite and ilmenite. Some of the basaltic samples possess amygdales filled with deuteroic calcites. The trachyandesites are porphyritic, with predominant phenocrysts of alkali feldspar and hornblende of 4–10 mm in grain size set in a matrix of fine-grained feldspar, clinopyroxene, hornblende and minor opaque oxides. The trachydacites occurring at the top of the profile are subaphyric, with minor phenocrysts like hornblende and plagioclase, as well as minor quartz. The groundmass is glassy with some fine-grained alkali feldspars and quartz.

ANALYTICAL TECHNIQUES

All the samples were crushed to millimeter-scale grain size after the removal of weathered rims and the rock chips were hand-picked using a magnifier to exclude the xenocrysts and amygdales. Only fresh xenocryst-free and amygdale-free rock chips were selected. These chips were first washed with purified water in an ultrasonic bath, then crushed in a tungsten-carbide jaw crusher. A split was finally ground to less than 160 mesh grain size in an agate ring mill, and this material was used for major and trace element analyses. The major element analysis was carried out using a wet chemical method at the Changsha Institute of Geotectonics, Chinese Academy of Sciences (CAS), with analytical errors of less than 1%.

Trace element abundances in the samples were determined using inductively coupled plasma–mass spectrometry (ICP–MS) at the Guiyang Institute of Geochemistry, CAS. The powders (about 100 mg) were placed in screw-top polytetrafluoroethylene (PTFE)-lined stainless steel bombs and dissolved by HF and HNO_3. The sealed bombs were placed in an electric oven and heated to 190°C for 12 h. Before carrying out ICP–MS, 1 p.p.m. Rh solution was added as an internal standard. The analytical errors were estimated to be less than 5% for elements that have a concentration greater than 10 p.p.m. and were about 10% for transition metals such as Cr, Ni, V and Sc from repetitive analyses of international standards of OU-3 (granite) and

AMH-1 (andesite). Duplicate runs gave a relative standard deviation (RSD) of less than 5% for most analyzed elements, except for transition metals, which generally gave an RSD of less than 10%. A detailed description of the analytical technique has been described by Qi *et al.* (2000).

K–Ar dating was performed at the Guangzhou Institute of Geochemistry, CAS. A detailed description of the sample preparation and analytical procedure has been reported by Fan *et al.* (2003). The age calculation parameters used in this study were: $K^{40} = 0.1167\%$, $K_e = 5.811 \times 10^{-11}$/y, $K_b = 4.962 \times 10^{-10}$/y. The analytical result for the Chinese hornblende standard ZBH-2506 was 132.3 ± 2.1 Ma ($n = 5$) (its recommended age is 132.0 Ma).

Sr and Nd isotopic ratios were measured at the Institute of Geology and Geophysics, CAS. Rock chips of less than 20 mesh were leached in purified 6 N HCl for 24 h at room temperature and then ground to less than 200 mesh in an agate ring mill and dissolved in Teflon bombs. The Sr and Nd isotopic ratios were normalized to $^{86}Sr/^{88}Sr = 0.1194$ and $^{146}Nd/^{144}Nd = 0.7219$, respectively. The La Jolla standard yielded $^{143}Nd/^{144}Nd = 0.511862 \pm 10$ ($n = 13$) and NBS987 gave $^{87}Sr/^{86}Sr = 0.710240 \pm 11$ ($n = 6$). Whole procedure blank is about $2–5 \times 10^{-10}$ g for Sr and less than 5×10^{-11} g for Nd. The analytical errors for the Sr and Nd isotopic ratios were given as 2σ. The $^{87}Rb/^{86}Sr$ and $^{147}Sm/^{144}Nd$ ratios were calculated using the Rb, Sr, Sm and Nd abundances obtained by ICP–MS. The $^{87}Sr/^{86}Sr(i)$ and $\varepsilon_{Nd}(t)$ were calculated using the K–Ar age of 105 Ma for the basaltic–andesitic rocks and 92 Ma for the felsic lavas, respectively.

RESULTS

VOLCANIC ERUPTION SEQUENCE IN THE LAIYANG BASIN

The four samples collected from the two profiles at the basin center were used to date the eruption episodes (Table 1). Two basaltic samples (97LW-3 and 97LW-17) from the base of the profiles yielded K–Ar ages of 105.1 ± 1.7 Ma and 106.5 ± 1.7 Ma, which are consistent with a K–Ar age of 105 Ma in the upper segment of basaltic lavas (Li & He 1997), but slightly younger than the Rb–Sr isochron age of 112 Ma of basalts from the lower segment of the Laiyang Basin (Qiu *et al.* 1996). Two felsic samples (97LW-13 and 97LW-50) from the top of the profiles gave K–Ar ages of 91.4 ± 1.5 Ma and 92.9 ± 1.5 Ma. It appears likely that the volcanic eruption spanned a range of 112–91 Ma, postdating the emplacement of voluminous granitoids and lamprophyres (130–120 Ma) and the associated large-scale gold mineralization event (125–120 Ma) by about 10 Ma (Guan *et al.* 1998; Wang *et al.* 1998; Yang & Zhou 2001; Guo *et al.* 2004).

ALTERATION

All the rock samples used for this study have experienced various degrees of alteration, as reflected by the high loss on ignition (LOI) that ranges from 0.7 to 8.1% (Table 2). The basaltic–andesitic rocks span an LOI range of 1.9–8.1%. During low-temperature hydrothermal alteration, the abundances of mobile elements like K, Na, Rb, Sr, Ba and U may be affected. However, in the Laiyang Basin volcanic rocks, only Sr shows a positive correlation with LOI, while other elements like K, Na, Rb and the measured $^{87}Sr/^{86}Sr$ ratio show a broad negative correlation with LOI (not shown in the paper). There is no correlation with LOI for Ba. Such variation in trends suggests that carbonation may have played a role after the eruption or formation of autogenetic carbonates during cooling of the igneous rock, as observed in the Sulu Belt lamprophyres (Guo *et al.* 2004). The weak correlation between MgO and Ni, and the negative correlation between Ni and SiO_2 (not shown in the paper) suggest selective Mg depletion during surface alteration. Although surface alteration weakly affected the behaviors of these mobile elements or isotopic ratios, we consider the variations in the characteristics of these elements in the Laiyang

Table 1 Results of K–Ar dating of Early Cretaceous volcanic rocks in the Laiyang Basin, eastern China

Sample	Rock type	Weight (g)	K_2O (wt%)	Total ^{40}Ar (10^{-10} mol/g)	Radiogenic ^{40}Ar (10^{-10} mol/g)	^{40}K (10^{-8} mol/g)	Age (Ma)
97LW-3	trachybasalt	0.064	1.59	2.985	2.179	4.746	105.1 ± 1.7
97LW-17	trachybasalt	0.046	1.93	3.672	2.607	5.760	106.5 ± 1.7
97LW-13	trachydacite	0.064	3.39	5.605	4.596	10.12	92.9 ± 1.5
97LW-50	trachydacite	0.075	3.57	5.803	4.874	10.66	91.4 ± 1.4

Table 2 Major and trace element compositions of Early Cretaceous volcanic rocks in the Laiyang Basin

Sample	Basaltic group (107–105 Ma)								
Rock type	97LW-1	97LW-3	97LW-6	97LW-7	97LW-16	97LW-17	97LW-20	97LW-21	97LW-24
SiO_2	48.80	50.70	55.96	48.74	54.18	54.44	55.04	54.50	57.50
Al_2O_3	16.41	17.27	15.41	17.41	15.98	17.77	15.55	17.27	17.05
Fe_2O_3	2.16	4.10	2.38	4.27	4.15	2.75	4.42	2.54	2.98
FeO	3.90	2.96	3.40	3.51	2.62	4.44	2.86	3.57	2.32
CaO	12.27	7.66	8.44	8.96	5.58	6.23	5.58	3.76	5.30
MgO	4.34	4.62	4.29	4.49	4.16	4.43	4.15	4.43	3.02
K_2O	2.10	2.11	2.49	1.94	3.57	2.58	2.50	2.84	2.18
Na_2O	3.36	3.49	2.96	3.26	3.88	3.25	3.33	4.14	3.46
MnO	0.11	0.08	0.09	0.09	0.09	0.07	0.09	0.07	0.08
TiO_2	0.99	1.01	0.78	1.11	1.10	1.11	1.12	0.89	1.13
P_2O_5	0.39	0.48	0.30	0.40	0.41	0.46	0.51	0.44	0.40
LOI	4.95	4.81	3.40	5.32	3.62	2.32	4.63	4.89	3.87
Total	99.78	99.29	99.90	99.50	99.34	99.85	99.78	99.34	99.29
Mg#	57	56	58	52	54	54	52	58	52
Sc	20	17	19	25	16	18	16	14	16
V	143	145	133	186	137	156	146	116	135
Cr	367	161	394	186	109	149	235	56	143
Ni	123	63	123	56	29	47	78	19	68
Rb	16.3	31.1	41.6	28.6	95.5	51.6	49.7	53.8	35.6
Sr	1081	1006	718	1006	801	921	712	613	841
Y	18.8	20.9	17.8	20.0	21.8	21.5	19.9	17.5	17.0
Zr	168	205	178	151	304	237	258	210	164
Nb	9.6	11.5	8.2	8.0	14.4	12.5	14.1	10.2	8.0
Ba	1361	1369	1508	1169	2483	1678	1457	1832	1455
Hf	4.35	5.18	4.64	3.86	8.02	6.23	6.58	5.43	4.28
Ta	0.47	0.59	0.46	0.36	0.85	0.64	0.73	0.53	0.43
Th	6.85	10.15	7.67	5.47	17.59	12.76	14.95	15.96	5.65
U	1.17	1.69	1.34	0.98	2.91	2.38	2.61	2.65	1.01
La	57.96	67.39	57.37	53.67	85.16	72.93	69.91	88.40	43.28
Ce	105.6	122.9	103.4	98.96	154.3	133.4	129.0	153.4	78.73
Pr	11.72	13.29	11.15	10.88	16.39	14.15	13.76	15.77	8.60
Nd	42.52	48.30	40.54	40.66	56.88	51.83	49.12	54.63	32.52
Sm	6.82	7.42	6.58	6.53	8.80	8.09	7.65	7.98	5.84
Eu	2.05	1.89	1.78	1.97	2.10	2.14	1.87	2.28	1.75
Gd	5.13	5.73	5.11	5.05	6.39	5.62	5.50	5.45	4.41
Tb	0.70	0.78	0.65	0.73	0.88	0.84	0.76	0.73	0.61
Dy	4.10	4.22	3.46	4.22	4.66	4.54	4.19	3.64	3.47
Ho	0.72	0.78	0.66	0.81	0.87	0.87	0.76	0.70	0.68
Er	1.93	2.22	1.91	2.09	2.37	2.25	2.23	1.89	1.73
Tm	0.23	0.28	0.24	0.28	0.34	0.31	0.30	0.25	0.23
Yb	1.76	1.99	1.73	2.02	2.26	2.28	1.96	1.65	1.59
Lu	0.25	0.30	0.24	0.31	0.37	0.34	0.30	0.26	0.25

Sample	Basaltic group (107–105 Ma)							
Rock type	97LW-27	97LW-28	97LW-29	97LW-31	97LW-33	97LW-34	97LW-37	97LW-39
SiO_2	54.12	51.64	52.64	48.58	50.84	50.92	47.22	52.36
Al_2O_3	19.26	16.20	16.41	15.98	16.20	16.62	17.34	15.34
Fe_2O_3	0.18	3.02	3.46	2.03	4.02	0.37	3.17	2.67
FeO	6.10	3.30	2.28	4.68	2.83	5.93	4.45	3.85
CaO	6.21	7.46	7.20	6.67	9.38	8.26	9.97	8.26
MgO	5.28	3.58	2.45	6.55	2.64	3.49	5.70	3.39
K_2O	2.00	2.20	2.87	2.23	2.40	2.49	1.68	2.35
Na_2O	3.29	3.72	3.77	3.00	3.11	3.18	2.86	3.05
MnO	0.12	0.09	0.09	0.08	0.12	0.10	0.13	0.06
TiO_2	1.17	1.18	1.17	1.01	1.06	1.14	1.23	0.95
P_2O_5	0.42	0.60	0.59	0.49	0.44	0.45	0.46	0.43
LOI	1.94	6.82	6.43	8.10	6.56	6.25	5.35	6.65
Total	100.09	99.81	99.36	99.40	99.60	99.20	99.56	99.36

Table 2 *Continued*

Sample	Basaltic group (107–105 Ma)							
Rock type	97LW-27	97LW-28	97LW-29	97LW-31	97LW-33	97LW-34	97LW-37	97LW-39
Mg#	60	52	45	64	42	50	58	49
Sc	17	16	17	19	19	21	21	18
V	140	116	117	153	155	178	158	132
Cr	155	248	265	219	304	348	356	349
Ni	93	128	139	83	129	138	159	147
Rb	23.0	26.3	45.3	46.6	73.7	82.4	23.9	40.2
Sr	769	828	814	1326	817	899	818	1278
Y	18.3	22.4	22.0	18.7	22.6	21.7	20.8	18.9
Zr	169	247	237	166	291	317	176	192
Nb	8.7	15.9	14.3	9.7	14.5	15.8	11.8	10.7
Ba	1455	1369	1738	2307	1512	1656	1385	1658
Hf	4.46	6.19	6.21	4.36	7.57	8.13	4.46	4.76
Ta	0.46	0.78	0.74	0.49	0.75	0.82	0.62	0.58
Th	5.94	6.19	6.04	9.28	17.94	19.64	6.60	7.28
U	1.05	1.04	1.01	1.49	3.28	3.72	1.02	1.36
La	43.37	66.06	65.00	68.59	81.39	83.61	53.26	61.36
Ce	81.19	120.7	118.9	123.5	150.7	154.7	100.2	111.8
Pr	8.97	13.33	12.88	13.48	16.38	16.64	10.82	12.29
Nd	34.19	48.53	47.17	48.85	56.92	58.39	41.25	44.63
Sm	5.61	7.84	7.50	7.81	8.65	8.92	6.84	7.05
Eu	1.85	2.27	2.30	2.11	2.16	2.23	2.17	1.95
Gd	4.74	6.33	6.14	5.91	6.44	6.44	5.66	5.38
Tb	0.68	0.84	0.88	0.78	0.89	0.88	0.81	0.72
Dy	3.66	4.49	4.66	3.98	4.86	4.88	4.59	4.15
Ho	0.76	0.89	0.90	0.72	0.88	0.88	0.82	0.74
Er	1.95	2.35	2.22	2.04	2.37	2.43	2.27	2.13
Tm	0.25	0.29	0.30	0.24	0.35	0.35	0.30	0.26
Yb	1.79	2.02	2.02	1.71	2.23	2.20	2.04	1.86
Lu	0.26	0.33	0.31	0.26	0.36	0.33	0.31	0.26

Sample	Felsic group (93–91 Ma)								
Rock type	97LW-8	97LW-9	97LW-11	97LW-13	97LW-14	97LW-47	97LW-48	97LW-50	97LW-54
SiO_2	59.72	59.98	59.32	60.42	60.20	64.24	62.72	64.78	60.40
Al_2O_3	16.41	16.98	17.34	17.27	16.05	16.84	16.91	16.70	17.55
Fe_2O_3	1.76	1.84	1.98	1.97	2.33	2.89	2.01	3.46	2.98
FeO	2.20	2.34	2.06	2.00	1.82	0.61	0.98	0.63	1.30
CaO	4.54	3.96	4.35	4.87	4.28	3.43	4.43	3.24	4.49
MgO	1.46	1.13	1.23	1.04	1.08	1.51	1.98	1.63	2.55
K_2O	3.51	3.99	3.83	3.84	3.86	3.73	3.36	3.88	3.30
Na_2O	3.71	3.86	3.90	3.74	4.17	4.30	4.39	4.21	4.23
MnO	0.11	0.09	0.10	0.10	0.10	0.04	0.06	0.03	0.07
TiO_2	0.43	0.52	0.52	0.50	0.52	0.84	0.78	0.83	0.83
P_2O_5	0.30	0.30	0.31	0.29	0.32	0.32	0.23	0.24	0.34
LOI	5.92	4.45	5.02	4.61	4.61	1.49	2.53	0.69	2.00
Total	100.07	99.44	99.96	100.65	99.34	100.24	100.38	100.32	100.04
Mg#	41	34	37	33	33	46	56	44	54
Sc	5	5	5	5	5	10	10	10	11
V	42	45	44	45	45	69	69	74	88
Cr	11	7	6	10	10	61	81	66	115
Ni	4	4	4	5	5	25	41	19	51
Rb	72.5	94.8	90.0	97.6	86.5	97.5	97.0	109	85.0
Sr	739	769	871	789	724	719	617	602	782
Y	14.7	15.6	15.6	15.4	15.3	18.0	17.1	15.9	15.8
Zr	143	147	148	146	138	258	250	258	211
Nb	9.7	10.5	10.0	10.1	9.8	11.6	10.9	11.8	9.4
Ba	2288	2795	2397	2978	2913	1982	1525	2049	2146
Hf	3.75	4.09	4.25	4.26	4.52	7.46	6.88	7.34	5.65
Ta	0.49	0.57	0.57	0.54	0.57	0.69	0.65	0.67	0.57
Th	15.05	16.00	16.20	16.71	16.04	18.21	18.50	20.40	13.96
U	2.34	2.31	2.38	2.51	2.23	2.51	3.04	3.05	2.77
La	83.02	87.42	87.69	88.50	85.73	81.23	74.37	78.05	65.64

Table 2 *Continued*

Sample	Felsic group (93–91 Ma)								
Rock type	97LW-8	97LW-9	97LW-11	97LW-13	97LW-14	97LW-47	97LW-48	97LW-50	97LW-54
Ce	138.6	146.4	147.2	149.2	142.5	146.2	132.6	138.1	118.3
Pr	13.77	14.50	14.68	14.47	14.34	15.11	13.88	14.15	12.12
Nd	44.96	47.78	47.48	47.70	46.92	52.48	46.31	47.69	42.29
Sm	5.95	6.19	6.54	6.44	6.73	7.04	6.71	6.87	6.95
Eu	1.66	1.78	1.84	1.76	1.68	1.72	1.55	1.65	1.78
Gd	4.38	4.57	4.52	4.70	4.43	5.60	4.96	4.71	4.75
Tb	0.55	0.59	0.60	0.58	0.57	0.74	0.63	0.66	0.62
Dy	2.87	3.05	3.16	3.14	3.07	3.70	3.63	3.55	3.11
Ho	0.53	0.57	0.61	0.59	0.55	0.74	0.67	0.68	0.62
Er	1.55	1.66	1.62	1.53	1.65	1.95	1.82	1.70	1.77
Tm	0.23	0.22	0.25	0.26	0.22	0.29	0.22	0.25	0.22
Yb	1.41	1.57	1.60	1.57	1.40	1.57	1.68	1.63	1.43
Lu	0.25	0.24	0.26	0.23	0.25	0.26	0.26	0.21	0.24

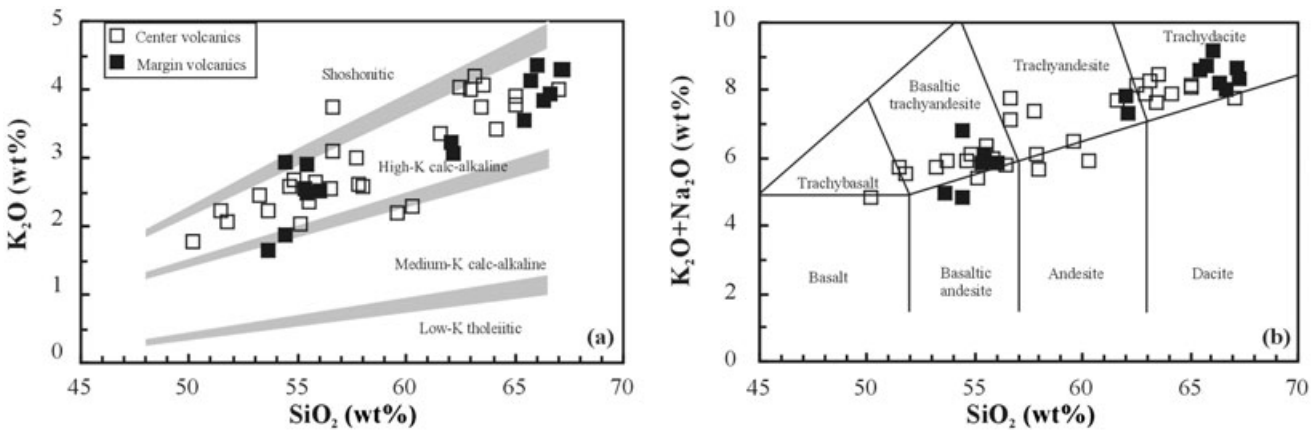

Fig. 3 (a) SiO_2 versus K_2O and (b) total alkalis versus SiO_2 (TAS) plots of Early Cretaceous volcanic rocks in the Laiyang Basin (reproduced from Middlemost 1994, with permission).

Basin volcanic rocks to mainly reflect the effect of magmatic processes rather than surface alteration.

MAJOR AND TRACE ELEMENTS

We divided the rocks into two groups, basaltic–andesitic and felsic, according to the spatial distribution, the eruption interval (>10 Ma) and the different lithology between the lower basaltic–andesitic and upper felsic lavas. The basaltic–andesitic rocks span an SiO_2 range of 51.0–59.6% and an MgO range of 2.6–7.2%. The felsic lavas have an SiO_2 range of 61.6–67.0% and an MgO range of 1.1–2.6%. All rocks have a high K_2O content (1.78–4.20%) and show high-K calc-alkaline affinities in an SiO_2 versus K_2O diagram (Middlemost 1994). In the total alkalis versus SiO_2 (TAS) figure (Fig. 3b), it can be seen that the rocks comprise a wide spectrum of rock types, ranging from trachybasalts, basaltic trachyandesites and trachyandesites, to trachydacites.

Relative to the basaltic–andesitic group, the felsic lavas generally have high concentrations of LREEs, Th (and U) and LILEs (e.g. K and Rb), and low concentrations of MgO, $FeO + Fe_2O_3$ (FeO_T), CaO, Sr, TiO_2, P_2O_5 and compatible elements like Cr, Ni, Sc and V (Table 2). In Figure 4a–f, both groups of rocks show a decrease in MgO, FeO_T and CaO concentrations and an increase in K_2O content (Fig. 3a) following an increase in SiO_2. The basaltic rocks show random variations in Al_2O_3, TiO_2 and P_2O_5 concentrations, but these generally decrease in the felsic group following magma evolution. In essence, there appear to be compositional gaps in FeO_T, TiO_2 and P_2O_5 between the two groups. Except for a few samples (e.g. 97LW-16), most of the basaltic–andesitic samples have low and weakly variable K_2O/P_2O_5 (3.7–5.6) and K_2O/TiO_2 (1.4–2.5) ratios relative to the

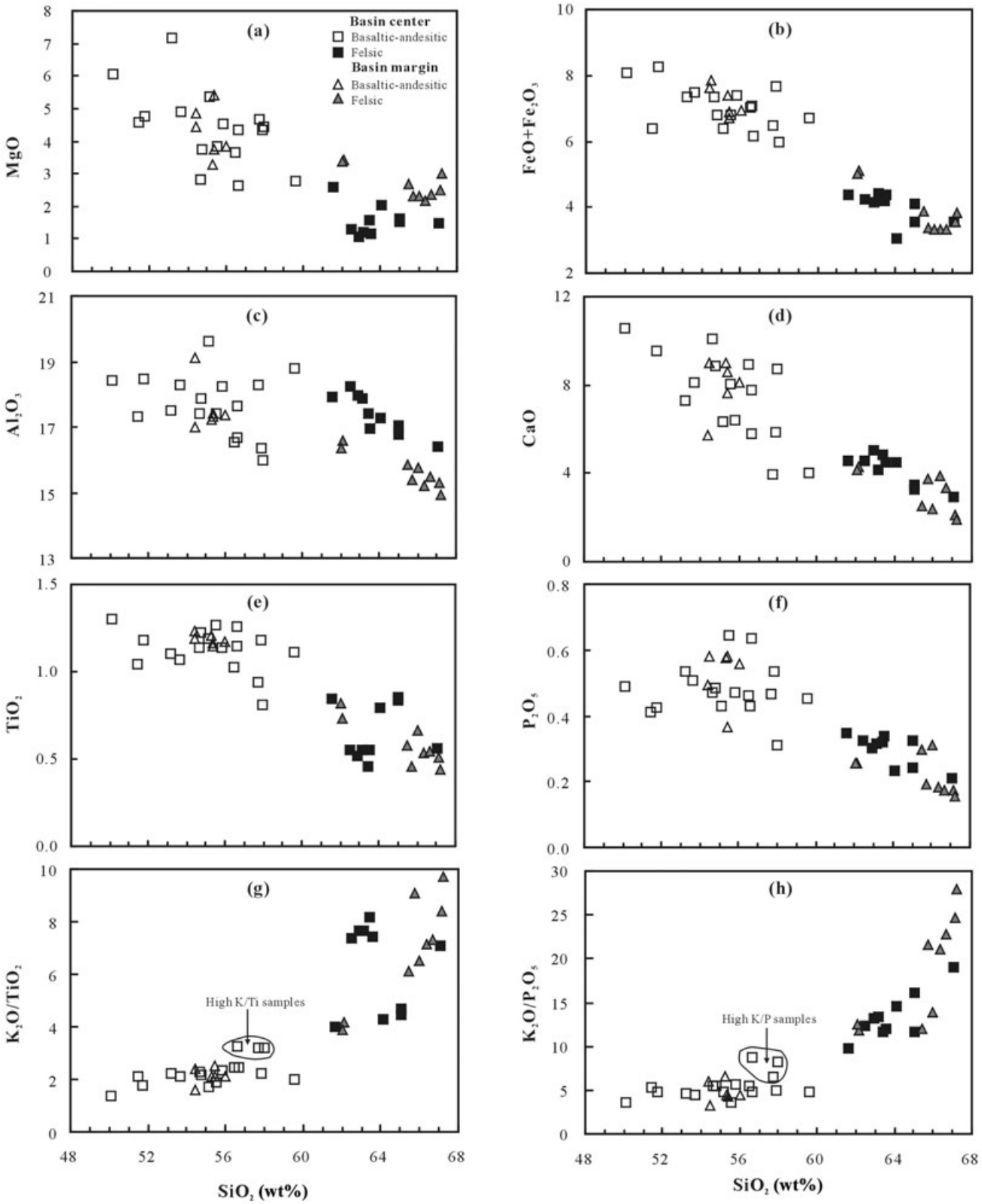

Fig. 4 Plots of SiO_2 versus major oxide content, as well as K_2O/TiO_2 and K_2O/P_2O_5 for Early Cretaceous volcanic rocks in the Laiyang Basin. (a) MgO; (b) FeO + Fe_2O_3; (c) Al_2O_3; (d) CaO; (e) TiO_2; (f) P_2O_5; (g) K_2O/TiO_2; and (h) K_2O/P_2O_5.

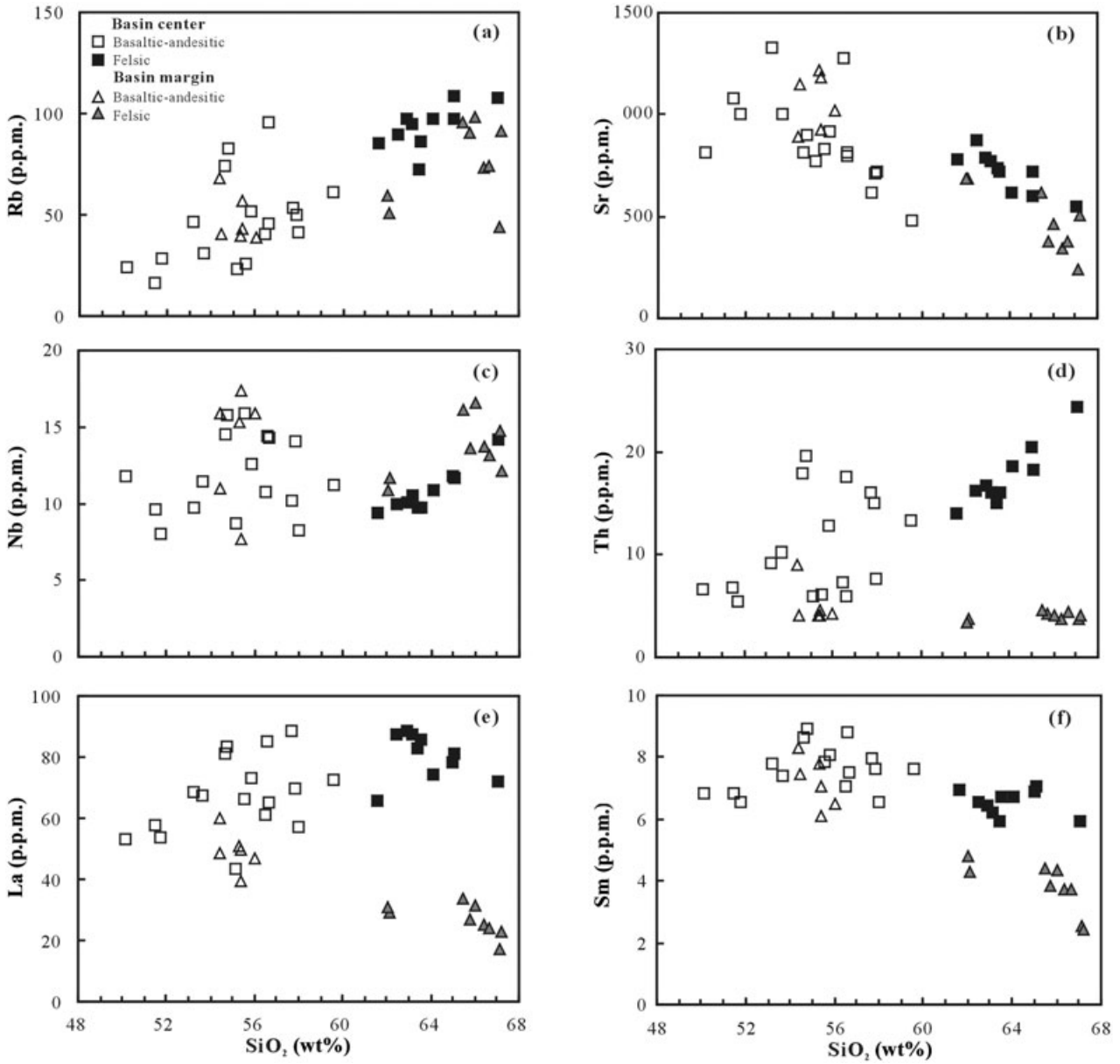

Fig. 5 Plots of SiO_2 versus trace element content for Early Cretaceous volcanic rocks in the Laiyang Basin. (a) Rb; (b) Sr; (c) Nb; (d) Th; (e) La; and (f) Sm.

felsic lavas, which have much higher and varied K_2O/P_2O_5 (9.7–19) and K_2O/TiO_2 (4.0–8.2) ratios.

As can be seen in Figure 5, both groups show a general increase in Rb and Th, and a decrease in Sr following magma evolution. The abundances of Nb and La in the basaltic–andesitic rocks are randomly variable, while in the felsic lavas, Nb shows a positive correlation with SiO_2 and a broad negative correlation with La. Middle rare earth elements (MREEs; e.g. Sm and Tb) exhibit different geochemical behaviors during the evolution of the basaltic–andesitic rocks. The Sm concentration first increases and then decreases following magma evolution, while a general decrease in Sm concentration is observed in the felsic rocks. Like the variation in the trends of the major elements, there is also a Sr gap in Figure 5b.

All rocks show strongly fractionated chondrite-normalized rare earth element (REE) patterns (La/Yb_{CN} = 16–36 and 18–41 in the basaltic–andesitic and felsic groups, respectively) with slightly negative Eu anomalies (Eu/Eu* = 0.82–1.07 and 0.71–0.98 in the basaltic–andesitic and felsic groups, respectively) (Fig. 6). Again, all rocks are characterized by strong LILE (e.g. Ba and K) and LREE enrichment with variable HFSE depletion in the primitive mantle (PM)-normalized spidergrams, similar to that of the Sulu Belt lamprophyres (Fig. 7). The Sr anomaly is variable in the basaltic–andesitic rocks, ranging from

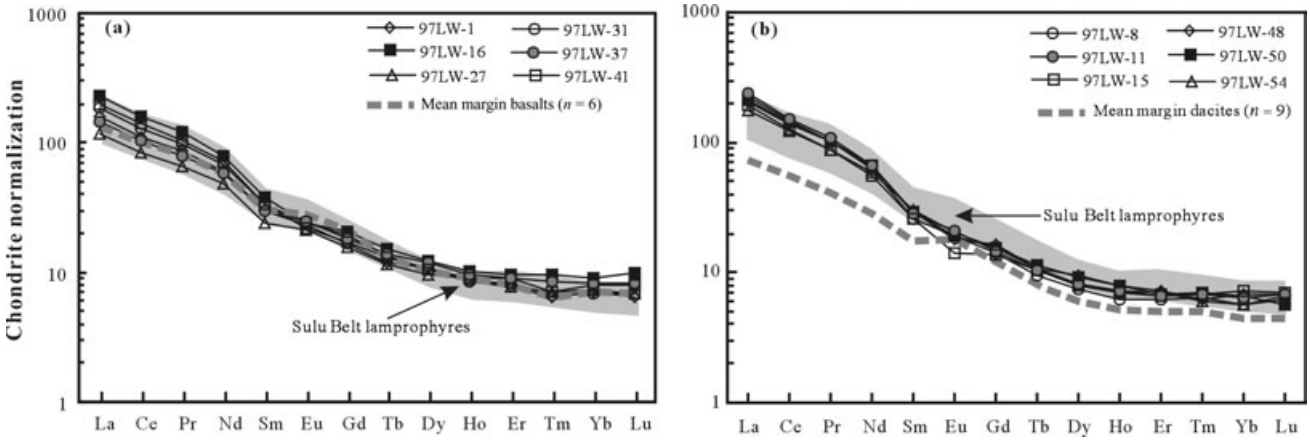

Fig. 6 Chondrite-normalized rare earth element (REE) patterns of Early Cretaceous volcanic rocks in the Laiyang Basin. Data for the Sulu Belt lamprophyres, margin volcanic rocks and chondrite are from Guo *et al.* (2004), Fan *et al.* (2001) and Taylor and McLennan (1985), respectively.

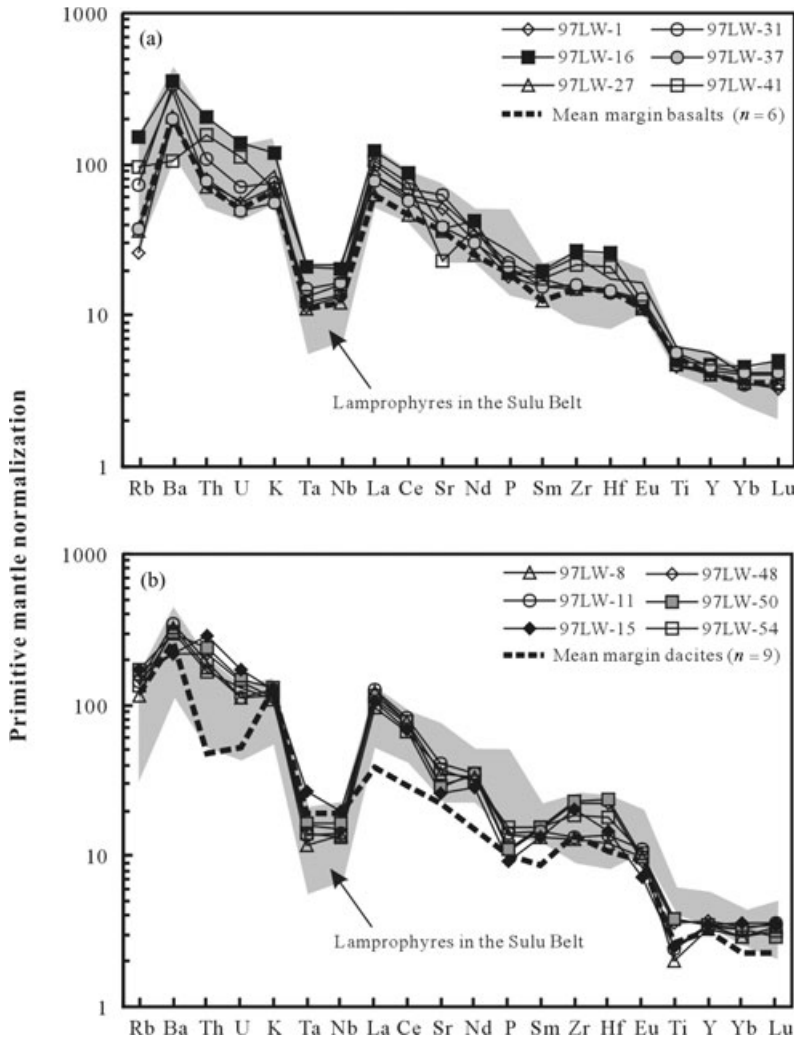

Fig. 7 Primitive mantle-normalized trace element spidergrams of Early Cretaceous volcanic rocks in the Laiyang Basin. Data for the Sulu Belt lamprophyres, margin volcanic rocks and primitive mantle are from Guo *et al.* (2004), Fan *et al.* (2001) and Sun and McDonough (1989), respectively.

slightly positive in high-Mg samples (e.g. 97LW-31) to negative in low-Mg rocks (e.g. 97LW-41), while a negative Sr anomaly is observed in all felsic rocks.

The basaltic–andesitic rocks exhibit similar Th/U, Zr/Nb and K/Rb ratios to their margin counterparts. Compared with the Sulu Belt lamprophyres, they show a higher K/Rb ratio, with similar Th/U

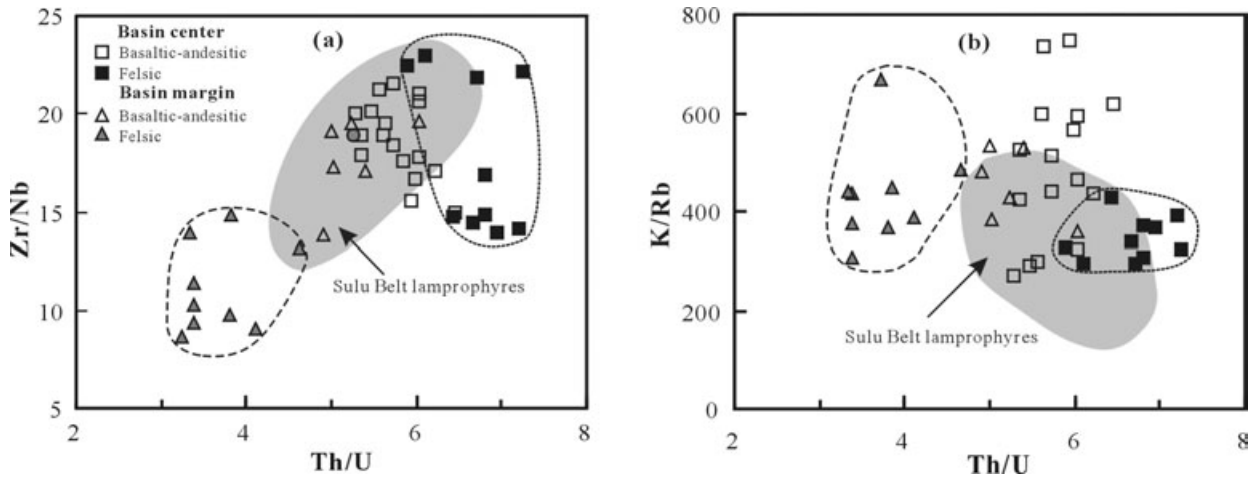

Fig. 8 Th/U versus (a) Zr/Nb and (b) K/Rb diagrams of Early Cretaceous volcanic rocks in the Laiyang Basin. Data for the Sulu Belt lamprophyres are from Guo *et al.* (2004), and for margin volcanic rocks, from Fan *et al.* (2001).

Table 3 Sr and Nd isotopic data for Early Cretaceous volcanic rocks in the Laiyang Basin, Sulu region

Sample	Rb (p.p.m.)	Sr (p.p.m.)	$^{87}Rb/^{86}Sr$	$^{87}Sr/^{86}Sr \pm 2\sigma$	$^{87}Sr/^{86}Sr(i)$	Sm (p.p.m.)	Nd (p.p.m.)	$^{147}Sm/^{144}Nd$	$^{143}Nd/^{144}Nd \pm 2\sigma$	$\varepsilon_{Nd}(t)$
97LW-3	31.1	1006	0.0896	0.708755 ± 20	0.70862	7.42	48.3	0.0929	0.511717 ± 14	–16.5
97LW-7	28.6	1006	0.0823	0.708494 ± 16	0.70837	6.53	40.7	0.0972	0.511705 ± 14	–16.8
97LW-16	95.5	801	0.3452	0.709827 ± 16	0.70931	8.80	56.9	0.0935	0.511645 ± 6	–17.9
97LW-17	51.6	921	0.1624	0.708831 ± 14	0.70859	8.09	51.8	0.0943	0.511712 ± 9	–16.6
97LW-20	49.7	712	0.2018	0.708643 ± 17	0.70834	7.65	49.1	0.0942	0.511699 ± 9	–16.9
97LW-27	23.0	769	0.0867	0.707628 ± 19	0.70750	5.61	34.2	0.0991	0.511770 ± 8	–15.6
97LW-28	26.3	828	0.0918	0.708407 ± 18	0.70827	7.84	48.5	0.0977	0.511661 ± 11	–17.7
97LW-31	46.6	1326	0.1017	0.709123 ± 13	0.70897	7.81	48.8	0.0966	0.511748 ± 8	–16.0
97LW-34	82.4	899	0.2653	0.708933 ± 19	0.70854	8.92	58.4	0.0923	0.511707 ± 10	–16.7
97LW-39	40.2	1278	0.0909	0.708539 ± 18	0.70840	7.05	44.6	0.0955	0.511727 ± 13	–16.4
97LW-9	94.8	769	0.3570	0.710780 ± 15	0.71031	6.19	47.8	0.0784	0.511630 ± 9	–18.0
97LW-13	97.6	789	0.3579	0.710763 ± 15	0.71030	6.44	47.7	0.0816	0.511631 ± 13	–18.0
97LW-15	117	549	0.5663	0.710311 ± 18	0.70957	5.91	38.9	0.0918	0.511666 ± 12	–17.5
97LW-48	97.0	617	0.4551	0.710508 ± 20	0.70991	6.71	46.3	0.0877	0.511648 ± 11	–17.8
97LW-50	109	602	0.5232	0.711769 ± 20	0.71109	6.87	47.7	0.0871	0.511579 ± 9	–19.1
97LW-54	85.1	782	0.3148	0.710496 ± 20	0.71008	6.95	42.3	0.0994	0.511661 ± 11	–17.7

The initial Sr and Nd isotopic data were calculated at 105 Ma and 92 Ma for the basaltic–andesitic and felsic groups, respectively.

and Zr/Nb ratios. The center felsic rocks have the highest Th/U ratio, and have a higher Zr/Nb ratio, but a lower K/Rb ratio than their margin counterparts (Fig. 8).

Sr–Nd ISOTOPES

The results of the Sr–Nd isotope analysis of 10 samples from the basaltic–andesitic group and six samples from the felsic group are shown in Table 3. The $^{87}Sr/^{86}Sr$ ratio for basaltic–andesitic rocks spans a relatively large range (0.707628–0.709827), but the $^{143}Nd/^{144}Nd$ ratio spans a limited range (0.511645–0.511770). The eruption age-corrected $^{87}Sr/^{86}Sr(i)$ ratio spans a range of 0.70750–0.70931 and the $\varepsilon_{Nd}(t)$ value ranges from –17.9 to –15.6, similar to the Early Cretaceous Sulu Belt lamprophyres. There is a broad negative correlation between $^{87}Sr/^{86}Sr(i)$ and $\varepsilon_{Nd}(t)$ (Fig. 9). The highly radiogenic Sr and non-radiogenic Nd isotopic compositions are completely different from the Cenozoic xenolith-bearing alkaline basalts (Zhi *et al.* 1994). Compared with the basaltic–andesitic rocks, the felsic lavas have an even higher $^{87}Sr/^{86}Sr$ ratio (0.710311–0.711769) and a lower $^{143}Nd/^{144}Nd$ ratio (0.511579–0.511666), with the $^{87}Sr/^{86}Sr(i)$ ratio ranging from 0.70957 to 0.71109 and $\varepsilon_{Nd}(t)$ ranging from –19.1 to –17.5. Compared with their margin counterparts (Fan *et al.* 2001), both the basaltic–andesitic and felsic groups from the basin center have slightly higher $^{87}Sr/^{86}Sr(i)$ values at corresponding $\varepsilon_{Nd}(t)$ values.

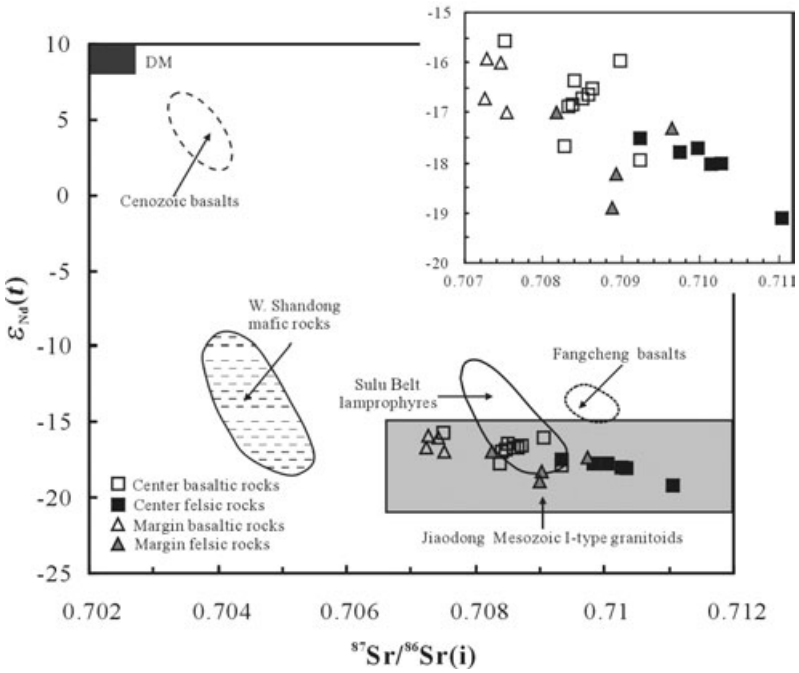

Fig. 9 Sr and Nd isotope diagram of Early Cretaceous volcanic rocks in the Laiyang Basin. Data are from Guo *et al.* 2004 (Sulu Belt lamprophyres); Zhao *et al.* 1997, Zhou & Lü 2000 and Zhou *et al.* 2002 (Mesozoic granites in the Jiaodong region); Zhang *et al.* 2002 (Fangcheng basalts); Guo *et al.* 2003 (mafic rocks in West Shandong province); Fan *et al.* 2001 (margin volcanic rocks); and Zhi *et al.* 1994 (Cenozoic xenolith-bearing basalts). DM, depleted mantle.

DISCUSSION

The eruption interval (>10 Ma) and compositional gaps in some elements (e.g. FeO_T, TiO_2, P_2O_5 and Sr) between the basaltic–andesitic and felsic groups tend to suggest that both groups cannot be generated through the simple fractional crystallization of a common primary melt. In the following section, we will discuss the petrogeneses of the two groups and their relationship with the tectonic evolution of the Sulu Belt.

PETROGENESIS OF THE BASALTIC–ANDESITIC GROUP

Most of the basaltic–andesitic rocks in the Laiyang Basin have an Mg# (<60; Mg# = Mg/(Mg + ΣFe) in the atomic ratio) and Cr (56–394 p.p.m.) and Ni (19–159 p.p.m.) concentrations that are too low for them to represent primary magmas (Hart & Davis 1978; Baker *et al.* 1997). They are evolved melts, which have undergone differentiation en route to the surface. Hence, we will focus on the effect of magmatic processes and source characteristics on the evolution of these rocks.

MAGMA MIXING OR CRUST CONTAMINATION

The Laiyang Basin basaltic–andesitic rocks show moderate compositional ranges, variable LREE/HFSE (e.g. La/Nb = 4.2–8.7) and LILE/HFSE (e.g. Ba/Nb = 66–237) ratios, and highly radiogenic Sr and non-radiogenic Nd isotopic data. Such features in basaltic rocks might be caused by either magma mixing or crust contamination. Magma mixing is a likely cause of the systematic geochemical variations in the basaltic–andesitic magmas. For instance, a general decrease in MgO, FeO_T, CaO and Sr concentrations and an increase in Th, Rb and K_2O concentrations are accompanied by an increase in SiO_2 concentration. However, compositional variations for some other elements cannot be reconciled with a simple magma-mixing hypothesis. Concentrations of P_2O_5, TiO_2, Nb and Y, for example, reach their maximum in some of the samples at an SiO_2 composition of 55–57%. In addition, the lack of mafic enclaves in the more evolved rocks also precludes magma mixing playing a significant role. Furthermore, as shown in the SiO_2 versus $^{87}Sr/^{86}Sr(i)$ and $\varepsilon_{Nd}(t)$ diagrams (Fig. 10), there is no clear magma-mixing trend between the basaltic–andesitic and felsic groups. Thus, a simple binary magma-mixing model seems unsuitable for explaining the geochemical variations in these rocks.

Alternatively, crust contamination, or assimilation and fractional crystallization (AFC), can be an effective cause of Sr–Nd isotopic variations and LILE and LREE enrichment relative to HFSE enrichment in the evolved magmas. Mass balance considerations suggest that features such as high Ba/Nb (66–238) and La/Nb (4.2–8.7) ratios and highly radiogenic Sr, but non-radiogenic Nd, isotopic compositions in the basaltic–andesitic rocks cannot realistically be attributed to crust contam-

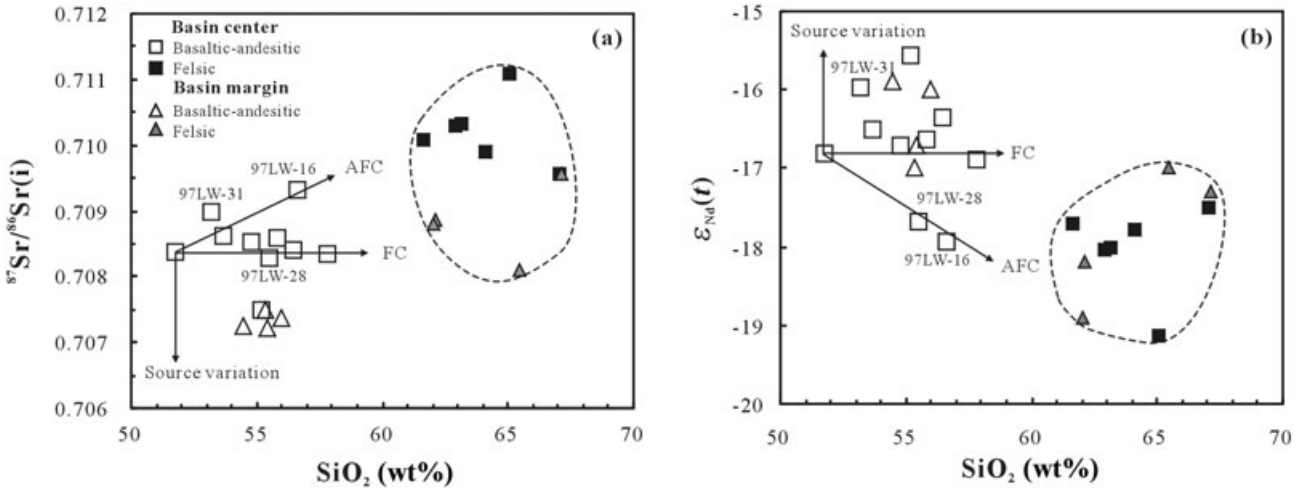

Fig. 10 SiO_2 versus (a) $^{87}Sr/^{86}Sr(i)$ and (b) $\varepsilon_{Nd}(t)$ diagrams, showing the possible magmatic processes that are predominant during the magma evolution. AFC, assimilation and fractional crystallization; FC, fractional crystallization.

ination of mid-oceanic ridge basalt (MORB), oceanic island basalt (OIB) or other low La/Nb ratio magmas (Hawkesworth *et al.* 1995; Jahn *et al.* 1999; Fan *et al.* 2001). High Ba/Nb and La/Nb ratios are widely ascribed to the source characteristics of a continental mantle lithosphere. However, crustal rocks have a high K_2O concentration relative to TiO_2 and P_2O_5 concentrations, and thus have high K_2O/TiO_2 and K_2O/P_2O_5 ratios, especially the felsic rocks in the upper middle crust. If crust contamination occurs, the contaminated magmas will possess high K_2O/TiO_2 and K_2O/P_2O_5 ratios. In the basaltic–andesitic group, there are indeed a few samples (e.g. 97LW-16) that have higher K_2O/TiO_2 (3.2) and K_2O/P_2O5 (8.7) ratios, with the highest $^{87}Sr/^{86}Sr(i)$ ratio being 0.70931, and the lowest $\varepsilon_{Nd}(t)$ value being –17.9, suggesting that crust contamination did play a role in their origination. The effect of crust contamination on this sample is also significant in the SiO_2 versus $^{87}Sr/^{86}Sr(i)$ and $\varepsilon_{Nd}(t)$ diagrams (Fig. 10), in which a clear AFC trend can be seen. Other samples show slightly varied K_2O/TiO_2 (1.4–2.5) and K_2O/P_2O_5 (3.7–5.6) ratios despite the shift in SiO_2 concentration, thus avoiding significant crust contamination. Similarly, in the SiO_2 versus $^{87}Sr/^{86}Sr(i)$ and $\varepsilon_{Nd}(t)$ diagrams (Fig. 10), these rocks show either a fractional crystallization (FC) trend of primary melts or a trend of source variation inherited from mantle heterogeneity. In summary, crust contamination may have played an important role in a few of the samples (e.g. 97LW-16) in elevating the K_2O/TiO_2, K_2O/P_2O_5 and $^{87}Sr/^{86}Sr(i)$ ratios, and lowering the Nd isotopic ratio, but the majority of the basaltic–andesitic rocks avoided significant contamination en route to the surface.

FRACTIONAL CRYSTALLIZATION

As discussed above, neither magma mixing nor crust contamination is applicable in interpreting the geochemical and isotopic variations in most of the basaltic–andesitic samples. Thus, variations in major and trace element compositions might be attributed to the different degrees of partial melting or fractional crystallization. Compared with the variable LILE/HFSE and LREE/HFSE ratios in the samples, the limited range of the La/Sm ratio, especially for samples with an SiO_2 concentration lower than 56% (an La/Sm range of 5.0–6.1), may suggest the importance of the role played by fractional crystallization during magma evolution.

Following the increase in concentration of SiO_2, the rapid decrease in the concentrations of MgO (Fig. 4a), FeO* and compatible elements such as Cr (56–394 p.p.m.), Ni (19–159 p.p.m.) and V (42–186 p.p.m.) indicates significant fractional crystallization of ferromagnesian minerals, such as olivine (Ol), orthopyroxene (Opx) and clinopyroxene (Cpx). The general decrease in Al_2O_3 concentration and variable Sr anomalies in the spidergrams following magma evolution indicate plagioclase (Pl) fractionation, consistent with the slightly negative Eu anomalies in some of the samples.

In contrast to other ferromagnesian minerals that generally have low REE partition coefficients, hornblende (Hb) is characterized by high MREE partition coefficients (Pearce & Norry 1979; Francis & Ludden 1995); thus, its fractionation will lead to an MREE decrease and convex REE patterns in the evolved magmas. In the basaltic–andesitic group, hornblende fractionation is insignificant

for samples with an SiO_2 concentration lower than 55%, but it is significant for the evolved samples with an SiO_2 concentration range of 55–60%, which explains the decrease in MREE concentration (e.g. Sm). In addition, the slightly varied P_2O_5 and TiO_2 concentrations suggest the insignificant role played by the fractional crystallization of accessories like apatite and ilmenite. Collectively, a fractional assemblage of Ol/Opx + Cpx + Pl ± Hb may be responsible for the element variations in most of the basaltic–andesitic lavas.

SOURCE CHARACTERISTICS

In order to characterize the source region for the basaltic rocks, the following discussion will be focused on the samples which have avoided crust contamination. The strong LILE and LREE enrichment, high HFSE depletion and highly radiogenic Sr and non-radiogenic Nd isotopic features in these rocks suggest that they were derived from an enriched mantle source that was either developed by time-integrated LILE and LREE enrichment or modified by recycled ancient crustal rocks (Jahn *et al.* 1999; Fan *et al.* 2001; Zhang *et al.* 2002; Guo *et al.* 2004).

The similarities in trace element geochemistry and Sr–Nd isotopic data between the basaltic–andesitic lavas and the Sulu Belt lamprophyres suggest that they have similar mantle sources. Based on the highly radiogenic Sr and non-radiogenic Nd isotopic data in the Early Cretaceous mafic rocks along the Dabie–Sulu Belt, many researchers considered the lithospheric mantle beneath the collisional belt to have been formed by the interaction between the subducted continental crust of the Yangtze affinities and the upper mantle above the subducted slab (Jahn *et al.* 1999; Fan *et al.* 2001; Zhang *et al.* 2002; Guo *et al.* 2004). For instance, in accordance with the moderate Zr/Hf and Nb/Ta fractionations in the Sulu Belt lamprophyres, Guo *et al.* (2004) postulated a carbonate- and rutile-rich melt metasomatism in response to the break-off of the subducted slab. Fan *et al.* (2001) interpreted the highly radiogenic Sr and non-radiogenic Nd isotopic compositions in the basaltic lavas along the Sulu Belt to be the result of the interaction between the lithospheric mantle and the subducted continental crust. Jahn *et al.* (1999) proposed a mixing model between the lower-middle crust and a depleted upper mantle to explain the origin of the Early Cretaceous ultramafic–mafic intrusions in the northern Dabie terrane. But it is not clear what kind of crustal rocks were involved in the formation of the enriched lithospheric mantle beneath the Dabie–Sulu Belt.

The low MgO affinity in the Laiyang Basin basaltic–andesitic rocks makes it difficult to directly characterize the source region because strong fractional crystallization might be a cause of the variations in LILE/HFSE and LREE/HFSE ratios. Here, we select two elemental pairs (e.g. Zr/Nb and Th/U) that were not much affected by fractionation of the Ol + Cpx + Hb + Pl assemblage. As discussed above, the limited range of the La/Sm value in these rocks suggest that the compositional range is mainly determined by the FC process instead of partial melting, so the two elemental ratios may reflect the source characteristics of the lithospheric mantle.

With regard to the PM (Sun & McDonough 1989), the mantle source for the Laiyang Basin basaltic–andesitic rocks has higher Th/U (5.3–6.5, with an average value of 5.7) and Zr/Nb (15–21, with an average value of 18) ratios, similar to that beneath the Sulu Belt (Fan *et al.* 2001; Guo *et al.* 2004). As can be seen in Figure 11, the broad increase in Th/U and Zr/Nb ratios toward higher Sr and lower Nd isotopic ratios suggests that the mantle sources have been modified by a component with high Th/U and Zr/Nb ratios, and extremely radiogenic Sr and non-radiogenic Nd isotopic features.

It has been documented that the abundances of heat production elements (HPEs), such as U and Th, decrease with depth in the crust as a result of the Earth's differentiation. For instance, granulite-facies metamorphism causes pervasive depletion of U ± Th because of the loss of grain boundary fluids and the breakdown of accessory phases at high P–T conditions, so the lower crust that is mainly composed of mafic granulite-facies rocks has low Th and U abundances and a low Th/U ratio relative to the upper middle crust (Rudnick & Fountain 1995). Zr and Nb are HFSEs and they are immobile during metamorphism, while Zr/Nb fractionation generally occurs in convergent plate margins, where residual rutile and other titanate minerals preferentially retain Nb from Zr and thus produce high Zr/Nb melts (Grove & Kinzler 1986; Arculus 1994; Foley *et al.* 2000); for example, modern intermediate-felsic arc volcanic rocks and Archean dioritic–tonalitic–trondhjemitic–granodioritic (DTTG) gneisses (Gao *et al.* 1999). However, evidence from the Dabie–Sulu Belt HP-UHP rocks indicated that the Yangtze continental crust had been subducted into the mantle during the Triassic collision between the two blocks (Li *et al.*

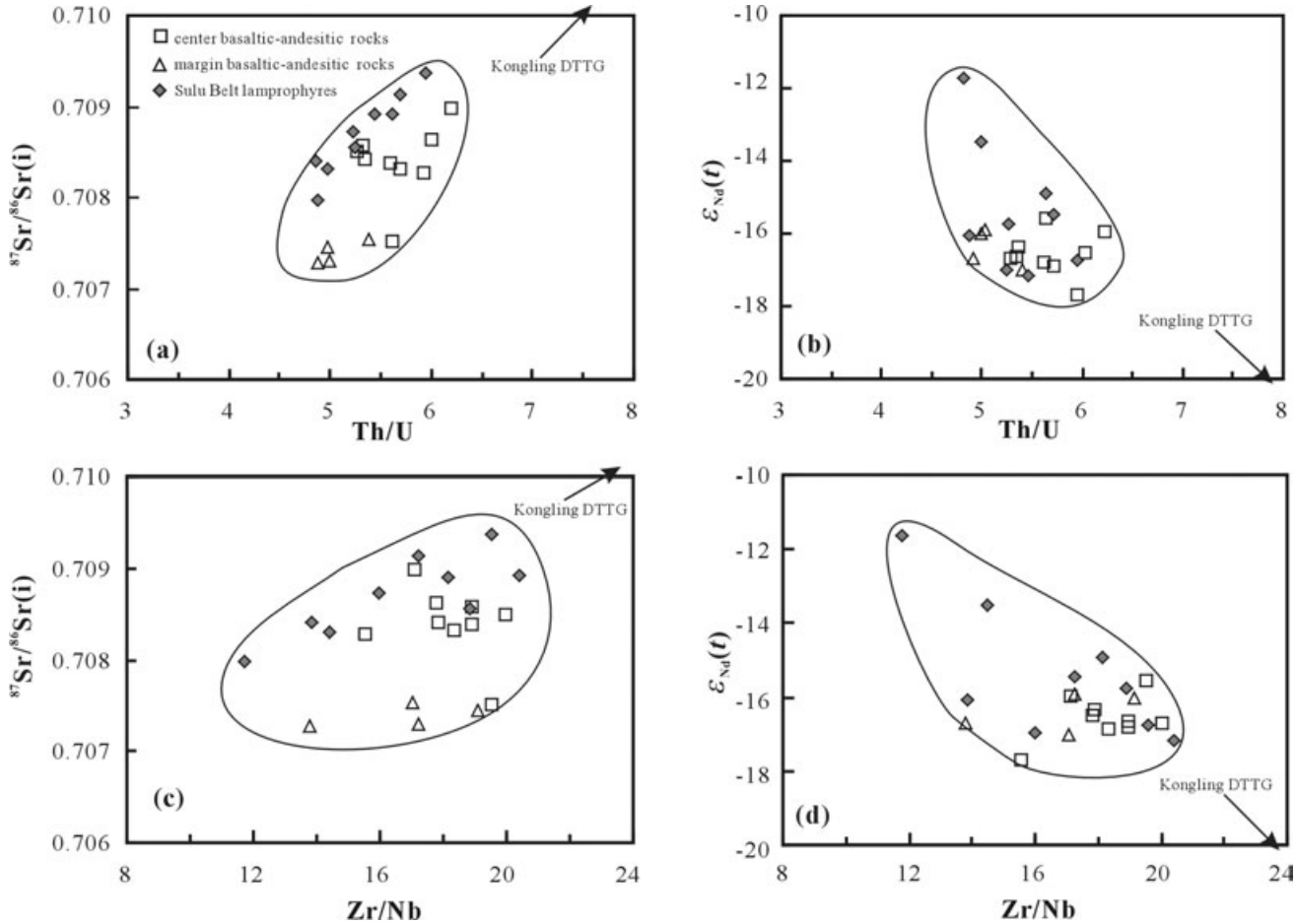

Fig. 11 (a),(b) Th/U versus Sr–Nd and (c),(d) Zr/Nb versus Sr–Nd isotope diagrams of Early Cretaceous mafic rocks in the Sulu Belt. These indicate a heterogeneously enriched mantle source modified by crustal rocks with high Th/U and Zr/Nb ratios, and extremely radiogenic Sr and low Nd isotopic data. Data are from Guo *et al.* 2004 (Sulu Belt lamprophyres); Fan *et al.* 2001 (margin volcanic rocks); and Gao *et al.* 1999 and Ma *et al.* 2000 (dioritic–tonalitic–trondhjemitic–granodioritic [DTTG] gneisses of the Kongling Group).

1993, 1999; Cong 1996; Jahn *et al.* 1996; Ye *et al.* 2000; Zheng *et al.* 2002). According to Gao *et al.* (1999) and Ma *et al.* (2000), the DTTG gneisses in the Kongling Group have developed extremely radiogenic Sr and non-radiogenic Nd isotopic compositions ($^{87}Sr/^{86}Sr(120\ Ma) = 0.710–0.719$; $\varepsilon_{Nd}(120\ Ma) = -47 \sim -25$), and high Th/U (8–11) and Zr/Nb (22–60) ratios. Hence, it appears likely that the Archean DTTG gneisses, such as the Archean high-grade metamorphic terrane represented by the Kongling Group in the YB (Gao *et al.* 1999; Ma *et al.* 2000), form the crustal component that is involved in the modification of the enriched lithospheric mantle (Fig. 11).

ORIGIN OF THE FELSIC LAVAS

Although there exist geochemical similarities between the basaltic–andesitic and felsic lavas at the basin center, we envisage a crustal origin for these felsic lavas on the following basis: (i) the compositional gaps (e.g. P, Sr and FeO_T) between them and the older basaltic–andesitic melts; (ii) the eruption gap (>10 Ma) between the two groups, the time span of which is too long for the fractional crystallization of primary basaltic magmas to produce their evolved felsic melts; (iii) the chemical composition, which is comparable with that of experimental slab melts (Rapp & Watson 1995); and (iv) similar Sr–Nd isotopic compositions to the I-type granitoids in the Sulu Belt that were previously considered as lower middle crustal melts (Zhao *et al.* 1997; Zhou & Lü 2000; Zhou *et al.* 2002).

Generation of high-K felsic volcanic rocks in orogenic belts is commonly attributed to the melting of crustal rocks in postcollisional/orogenic settings, as a consequence of decompression melting following the attenuation of the lithospheric root or slab break-off (Roberts & Clemens 1993; Davis & von Blanckenburg 1995; Altherr *et al.* 2000). Compared with their felsic counterparts along the basin mar-

gins, the center felsic lavas have higher Al_2O_3, Sr, REE and Th (U) concentrations, and higher molar $Al_2O_3/(MgO + FeO_T)$ and $CaO/(MgO + FeO_T)$, Th/U, Sr/Y and $^{87}Sr/^{86}Sr(i)$ ratios, with similar Nd isotopic data, but low MgO (also Mg#) concentration (Figs 4–8,11). Such compositional diversity between the two groups may be attributed to the different source compositions or the variation of melting conditions, such as H_2O content, pressure, temperature and oxygen fugacity (Wolf & Wyllie 1994; Gardien *et al.* 1995; Patiño Douce & Beard 1995, 1996; Thompson & Connolly 1995; Borg & Clynne 1998). However, the compositional differences could be produced by the partial melting of different source rocks, such as amphibolites, tonalitic gneisses, metagreywackes and metapelites under variable melting conditions. Results from partial melting experiments suggest that melts derived from metabasalts and andesites have lower molar $Al_2O_3/(MgO + FeO_T)$, but higher molar $CaO/(MgO + FeO_T)$ ratios than those derived from metapelites. As can be seen in Figure 12, one can draw the following conclusions about the origins of the center and margin felsic lavas:

1. The center felsic lavas have higher molar $Al_2O_3/(MgO + FeO_T)$ and $CaO/(MgO + FeO_T)$ ratios than their margin counterparts, overlapping the range of partial melts from metabasaltic and metatonalitic sources (Fig. 12a). This suggests that metaigneous rocks are predominant in the source. For the margin felsic lavas, the lower $Al_2O_3/(MgO + FeO_T)$ and $CaO/(MgO + FeO_T)$ ratios tend to indicate the presence of metasediments in the source.
2. The much higher Th (also U) abundance (Fig. 7) and Th/U ratio (Fig. 12b) in the center felsic

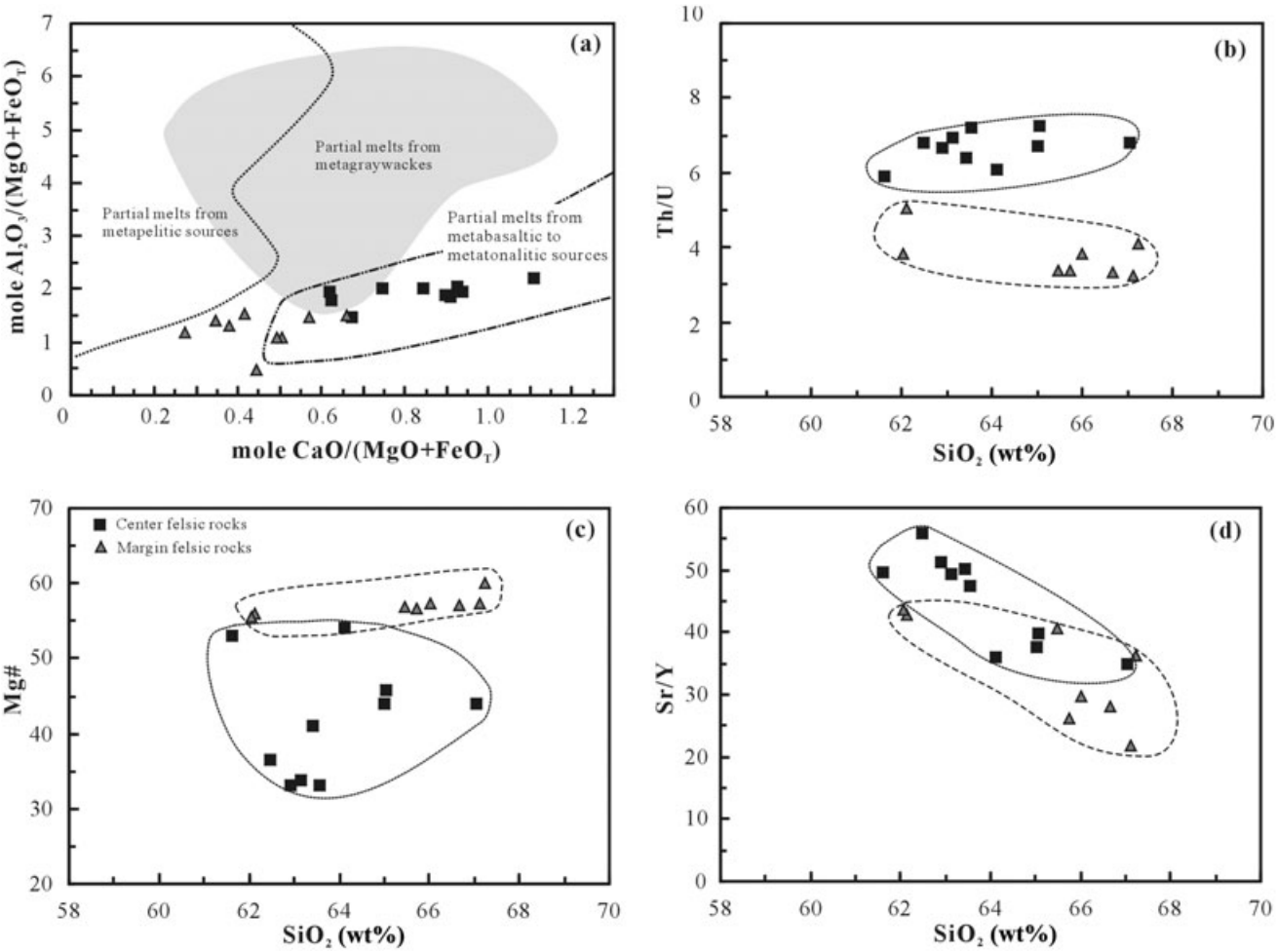

Fig. 12 Plots of (a) molar $CaO/(MgO + FeO_T)$ versus $Al_2O_3/(MgO + FeO_T)$, (b) SiO_2 versus Th/U, (c) SiO_2 versus Mg# and (d) SiO_2 versus Sr/Y of the felsic lavas for constraining the possible origins. Outlined fields in (a) denote the compositions of partial melts from experimental studies of the dehydration melting of various bulk compositions (Wolf & Wyllie 1994; Gardien *et al.* 1995; Patiño Douce & Beard 1995, 1996; Thompson & Connolly 1995). The lower Mg# of the center felsic lavas in (c) suggests shallower melting depths in magma genesis, consistent with their higher Th/U ratios in (b). The higher Sr/Y ratios of the center felsic lavas in (d) indicate that less residual plagioclase is required during melting compared to their marginal counterparts. See text for details.

lavas suggest that they were unlikely to be derived from granulite-facies protoliths that had low Th and U concentrations, while their margin felsic counterparts, with a lower Th (also U) concentration and Th/U ratio, favor source rocks predominantly with granulite-facies conditions. Additionally, with increasing pressure, the Mg# concentration of felsic partial melts increases relative to the magmas of coexisting garnet and biotite (Patiño Douce & Beard 1996). Thus, the center felsic magmas, with a lower Mg# concentration (Fig. 12c) than their margin counterparts, were generated at relatively shallower depths, and this is consistent with the higher Th (U) abundance and Th/U ratio in these rocks.

3. The higher Sr/Y ratios (Fig. 12d) in the center felsic rocks may suggest a lower amount of residual plagioclase during the melting process compared with their margin counterparts.
4. Both the center and margin felsic lavas in the Laiyang Basin generally have high Ba concentrations (1525–2978 p.p.m., with an average Ba concentration of 2261 p.p.m.). The origin of high-Ba granitoids, which are most common in Archean and Mesozoic terrains, can be related to the partial melting of Ba-enriched sources, such as OIBs, or the involvement of Ba-enriched mafic or carbonatitic melts (Tarney & Jones 1994). In the Sulu Belt, the widely distributed lamprophyres (120–127 Ma) and the evolved nature of the basaltic lavas imply the existence of coeval mafic accumulates beneath the belt, which can create Ba-enriched sources in the crust because all of their extrusive counterparts have high Ba concentrations.

IMPLICATIONS FOR TECTONIC EVOLUTION OF THE SULU BELT

High-K calc-alkaline rocks crop out widely in continental orogens in response to lithospheric extension induced by slab break-off (Davis & Blanckenburg 1995; Chen *et al.* 2003), convective thinning (England & Houseman 1989), gravitational collapse (Ruppel 1995) or lithospheric delamination (Bird 1979). They are believed to be melts of the metasomatized mantle lithosphere and/or the upwelling convective mantle, when the extent of lithospheric thinning is enough to cause the meeting of the geotherm and peridotite solidus (Mckenzie & Bickle 1988).

The similar geochemical and isotopic features among the center basaltic lavas, their margin counterparts and the Sulu Belt lamprophyres indicate that all these basaltic melts were derived from similar mantle sources that had been enriched in LILEs and LREEs. Thus, it is reasonable to conclude that the Wulian–Qingdao–Yantai Fault (F3) should not be considered as the lithospheric boundary between the NCB and YB. Because the metamorphic terranes around the fault have distinct ages, lithology and metamorphic history, it is likely that F3 acted as a detachment fault to separate the different terranes on the surface, as suggested by Li (1994), who proposed that the surface rocks with the Yangtze affinities in the Jiaodong region were overthrust on the NCB as a consequence of intracontinental compression and orogenism.

However, following the attenuation of the thickened lithosphere beneath the orogenic belt, passive rifting and asthenospheric upwelling occurred to trigger geothermal elevation from a cold and thickened lithosphere to a hot and rift-related one. Once the geotherm encountered the peridotite solidus, partial melting occurred to form the earlier calc-alkaline lamprophyres (Yang & Zhou 2001; Guo *et al.* 2004), but the majority of the mantle-derived melts were underplated into the lower middle crust, providing a large energy supply for the melting of the crustal rocks, such as the emplacement of the Kunyushan and Guojialing granites (Guan *et al.* 1998; Wang *et al.* 1998; Zhou & Lü 2000) and the associated large-scale gold mineralization in the Jiaodong region (Yang & Zhou 2001; Zhou *et al.* 2002). During this period, the extensional tectonics is characterized by crustal doming and orogenic uplifting, such as granitoid emplacement (Grimmer *et al.* 2003). As lithospheric attenuation continued, orogenic collapse and crustal rifting took place to form a relatively open system favorable for volcanic eruption and basin subsidence; for example, the Laiyang and Subei basins (Xu *et al.* 1987; Fan *et al.* 2001). Continuous heating caused by the thermal decay of the basaltic melts and crustal stretching then caused extensive remelting of the mixed source between the crustal rocks and the under-plated mafic rocks (e.g. lamprophyric melts) produced the younger high-Ba felsic lavas in the Laiyang Basin and along the Sulu Belt. Accordingly, the extensive eruption of the high-K calc-alkaline rocks in the Sulu Belt therefore favors an extensional regime as a result of the orogenic collapse following the progressive attenuation of the thickened lithosphere.

Available geochronological data from the Mesozoic igneous rocks in the Sulu Belt indicate pro-

longed magmatic episodes after the peak UHP metamorphism (Zhao *et al.* 1997; Guan *et al.* 1998; Wang *et al.* 1998; Zhou & Lü 2000; Chen *et al.* 2003). Taking into account the published data and the possible interpretations, we can summarize the general tectonic evolution of the Sulu collisional belt in the following five stages:

1. The peak HP-UHP metamorphism at *ca* 240 Ma occurred as a consequence of the subduction of the Yangtze continental crust and collision between the NCB and YB (Li *et al.* 1993; Ames *et al.* 1996; Zheng *et al.* 2002).
2. The break-off of the subducted slab at *ca* 225–205 Ma led to the retrogression and exhumation of the HP-UHP rocks and the emplacement of the Shidao potassic pyroxene diorite–syenite granitoid complex (Chen *et al.* 2003).
3. Intracontinental compression and orogeny started from *ca* 210 Ma and terminated by *ca* 160 Ma, characterized by the emplacement of peraluminous granitoids, such as the Linglong and Luanjiahe granites of 158–150 Ma (Wang *et al.* 1998; Zhou & Lü 2000).
4. Uplifting and crustal doming of the orogenic belt took place as a result of further attenuation of the thickened lithosphere at 130–120 Ma (Guan *et al.* 1998; Wang *et al.* 1998; Grimmer *et al.* 2003), resulting in extensive melting of the crust (e.g. the Kunyushan and Guojialing granites), and a lower extent of the enriched lithospheric mantle sources (for lamprophyres) and large-scale gold mineralization in the Jiaodong region (Yang & Zhou 2001; Guo *et al.* 2004).
5. The subsequent orogenic collapse (112–91 Ma) and formation of the Laiyang Fault basin (Qiu *et al.* 1996; Fan *et al.* 2001) triggered the extensive eruption of high-K calc-alkaline rocks and emplacement of A-type granites (Zhao *et al.* 1997).

CONCLUSIONS

Early Cretaceous high-K calc-alkaline volcanic rocks from the Laiyang Basin show variable LILE and LREE enrichment and HFSE depletion, and highly radiogenic Sr and non-radiogenic Nd isotopic features. They can be spatially and compositionally divided into two groups. The earlier basaltic–andesitic rocks, which have considerable geochemical and isotopic similarities with the Sulu Belt lamprophyres, suggest the presence of similar enriched mantle sources beneath the two tectonic units separated by F3. It is thus reasonable to conclude that the fault had acted as a surface detachment to separate the different terranes in the Jiaodong region instead of a lithospheric boundary between the NCB and YB. The younger felsic lavas, characterized by a low molar $Al_2O_3/(MgO + FeO_T)$ ratio but a high molar $CaO/(MgO + FeO_T)$ ratio, high Th/U ratios and high-Ba features, were derived from a mixed source comprising crustal metaigneous rocks and mafic accumulative counterparts of the basaltic and lamprophyric melts. The extensive eruption of Early Cretaceous high-K calc-alkaline volcanic rocks in the Sulu Belt thus favored an extensional regime in response to the progressive attenuation of the thickened lithosphere and orogenic collapse, as reflected in the development of the basin from a foreland basin (before the end of the Jurassic period) to a fault-rift basin (since the Early Cretaceous period).

ACKNOWLEDGEMENTS

We thank Mr L. Qi for his assistance in performing the ICP–MS analysis and R. H. Zhang for his help in analyzing the Sr and Nd isotopic data. The authors are also grateful to Mr Z. P. Pu for help with the K–Ar dating. The helpful suggestions provided by Professor Richard Arculus during the preparation of the manuscript are much appreciated. The thorough and constructive reviews and comments by two anonymous reviewers also helped to clarify the contents of the paper, which significantly improved the manuscript. Thanks are also due to the Associate Editor, Dr Yoji Arakawa, for his effort in editing this paper. This study was financially supported by the National Natural Science Foundation (40073011), Chinese Ministry of Science and Technology (G1999075504) and Chinese Academy of Sciences (KZCX1-107; GIGCX-04–04).

REFERENCES

ALDANMAZ E., PEARCE J. A., THIRLWALL M. F. & MITCHELL J. G. 2000. Petrogenetic evolution of late Cenozoic, post-collision volcanism in western Anatolia, Turkey. *Journal of Volcanology and Geothermal Research* **102**, 67–95.

ALTHERR P., HOLL A., HEGNER E., LANGER C. & KREUZER H. 2000. High-potassium, calc-alkaline I-type plutonism in the European Variscides: Northern Vosges (France) and northern Schwarzwald (Germany). *Lithos* **50**, 51–73.

AMES L., ZHO G. & XIONG B. 1996. Geochronology and isotopic character of high-pressure metamorphism with implications for collision of the Sino-Korean and Yangtze Cratons, central China. *Tectonics* **15**, 472–89.

ARCULUS R. J. 1994. Aspects of magma genesis in arcs. *Lithos* **33**, 189–208.

BAKER J. A., MENZIES M. A., THIRLWALL M. F. & MACPHERSON G. C. 1997. Petrogenesis of Quaternary intraplate volcanism, Sana'a, Yemen: Implications for plume–lithosphere interaction and polybaric melt hybridization. *Journal of Petrology* **38**, 1359–90.

BUREAU OF GEOLOGY AND MINERAL RESOURCES OF SHANDONG PROVINCE (BGMRS). 1991. *Regional Geology of Shandong Province*, pp. 1–594 (in Chinese). Geological Publishing House, Beijing.

BIRD P. 1979. Continental delamination and the Colorado Plateau. *Journal of Geophysical Research* **84**, 7561–71.

BORG L. E. & CLYNNE M. A. 1998. The petrogenesis of felsic calc-alkaline magmas from the southernmost Cascades, California: Origin by partial melting of basaltic lower crust. *Journal of Petrology* **39**, 1197–222.

CHEN J. F., XIE Z., LI H. M. *et al.* 2003. U–Pb zircon ages for a collision-related K-rich complex at Shidao in the Sulu ultrahigh pressure terrane, China. *Geochemical Journal* **37**, 33–46.

CHUNG S. L. 1999. Trace element and isotope characteristics of Cenozoic basalts around the Tanlu Fault with implications for the eastern plate boundary between North and South China. *Journal of Geology* **107**, 301–12.

CONG B. L. 1996. *Ultrahigh-Pressure Metamorphic Rocks in the Dabie–Sulu Region of China*, pp. 1–224. Science Press, Beijing and Kluwer Academic Publication, Dordrecht.

DAVIES J. H. & STEVENSON D. J. 1992. Physical model of source region of subduction zone volcanics. *Journal of Geophysical Research* **97**, 2037–70.

DAVIS J. H. & VON BLANCKENBURG F. 1995. Slab breakoff: A model of lithosphere detachment and its test in the magmatism and deformation of collisional orogens. *Earth and Planetary Science Letters* **129**, 327–43.

ENAMI M., SUZUKI K., ZHAI M. & ZHENG X. 1993. The chemical and Th-U-total Pb isochron ages of Jiaodong and Jiaonan metamorphic rocks in the Shandong Peninsula, eastern China. *Island Arc* **2**, 104–13.

ENGLAND P. C. & HOUSEMAN G. A. 1989. Extension during continental convergence, with application to the Tibet Plateau. *Journal of Geophysical Research* **94**, 17561–79.

FAN W. M., GUO F., WANG Y. J. & LIN G. 2003. Calc-alkaline volcanism of post-orogenic extension in the northern Da Hinggan mountains, northeastern China. *Journal of Volcanology and Geothermal Research* **121**, 115–35.

FAN W. M., GUO F., WANG Y. J., LIN G. & ZANG M. 2001. Post-orogenic bimodal volcanism along the Sulu orogenic belt in eastern China. *Physics and Chemistry of the Earth (a)* **27**, 733–46.

FAURE M., LIN W. & BRETON N. L. 2001. Where is the North China–South China block boundary in eastern China? *Geology* **29**, 119–22.

FOLEY S. F., BARTH M. G. & JENNER G. A. 2000. Rutile/melt partition coefficients for trace elements and an assessment of the influence of rutile on the trace element characteristics of subduction zone magmas. *Geochimica et Cosmochimica Acta* **64**, 933–48.

FRANCIS D. & LUDDEN J. 1995. The significance of hornblende in mafic alkaline lavas: A study in the northern Canadian Cordillera. *Journal of Petrology* **38**, 1171–91.

GAO S., LING W. L., QIU Y. M., ZHOU L., HARTMAN G. & SIMON K. 1999. Contrasting geochemical and Sm–Nd isotopic compositions of Archean metasediments from the Kongling high-grade terrain of the Yangtze Craton: Evidence for cratonic evolution and redistribution of REE during crustal anatexis. *Geochimica et Cosmochimica Acta* **63**, 2071–88.

GARDIEN V., THOMPSON A. B., GRUJIC D. & ULMER P. 1995. Experimental melting of biotite–plagioclase–quartz–muscovite assemblages and implications for crustal melting. *Journal of Geophysical Research* **100**, 15581–91.

GRIMMER J. C., RATSCHBACHER L., MCWILLIAMS M. *et al.* 2003. When did the ultrahigh-pressure rocks reach the surface? A $^{207}Pb/^{206}Pb$ zircon, $^{40}Ar/^{39}Ar$ white mica, Si-in-white mica, single-grain provenance study of Dabie Shan synorogenic foreland sediments. *Chemical Geology* **197**, 87–110.

GROVE T. L. & KINZLER R. J. 1986. Petrogenesis of andesites. *Annual Reviews to Earth and Planetary Science Letters* **14**, 417–54.

GUAN K., LUO Z. K., MIAO L. C. & HUANG J. Z. 1998. SHRIMP zircon chronology for Guojialing suite granite in Jiaodong Zhaoye district. *Scientia Geologica Sinica* **33**, 318–28 (in Chinese, with English abstract).

GUO F., FAN W. M., WANG Y. J. & LIN G. 2003. Geochemistry of late Mesozoic mafic magmatism in west Shandong Province, eastern China: Characterizing the lost lithospheric mantle beneath the North China Block. *Geochemical Journal* **37**, 63–77.

GUO F., FAN W. M., WANG Y. J. & ZHANG M. 2004. Origin of early Cretaceous calc-alkaline lamprophyres from the Sulu orogen in eastern China: Implications for enrichment processes beneath the continental collisional belt. *Lithos* **78**, 291–305.

HART S. R. & DAVIS K. E. 1978. Nickel partitioning between olivine and silicate melt. *Earth and Planetary Science Letters* **40**, 203–19.

HAWKESWORTH C. J., TURNER S., GALLAGHER K., HUNTER A., BRAHSHAW T. & ROGERS N. 1995. Calc-alkaline magmatism, lithospheric thinning and exten-

sion in the Basin and Range. *Journal of Geophysical Research* **100**, 10271–86.

ISHIZAKA K., HIRAJIMA T. & ZHENG X. 1994. Rb–Sr dating for the Jiaodong gneiss of the Su-Lu ultrahigh pressure province, eastern China. *Island Arc* **3**, 232–41.

JAHN B. M., CORNICHET J., CONG B. L. & YUI T. F. 1996. Ultrahigh-ε_{Nd} eclogites from an ultrahigh-pressure metamorphic terrane of China. *Chemical Geology* **127**, 61–79.

JAHN B. M., WU F. Y., LO C.-H. & TSAI C. H. 1999. Crust–mantle interaction induced by deep subduction of the continental crust: Geochemical and Sr–Nd isotopic evidence from post-collisional mafic–ultramafic intrusions of the northern Dabie complex, central China. *Chemical Geology* **157**, 119–46.

LI Z. X. 1994. Collision between the North and South China Blocks: A crustal-detachment model for suturing in the region east of the Tanlu Fault. *Geology* **22**, 739–42.

LI S. & HE W. 1997. Division and comparison of the Mesozoic strata in Shandong Province. *Geological Journal of China Universities* **3**, 87–93 (in Chinese, with English abstract).

LI S. G., JAGOUTZ E., LO C.-H., CHEN Y. Z. & LI Q. L. 1999. Sm/Nd, Rb/Sr and $^{40}Ar/^{39}Ar$ isotopic systematics of the ultrahigh-pressure metamorphic rocks in the Dabie–Sulu Belt, central China: A retrospective view. *International Geology Reviews* **41**, 1114–24.

LI S. G., XIAO Y. L., LIOU D. L. *et al.* 1993. Collision of the North China and Yangtze blocks and formation of coesite-bearing eclogites: Timing and process. *Chemical Geology* **109**, 89–111.

MA C. Q., EHLERS C., XU C. H., LI Z. C. & YANG K. G. 2000. The roots of the Dabieshan ultrahigh-pressure metamorphic terrane: Constraints from geochemistry and Nd–Sr isotope systematics. *Precambrian Research* **102**, 279–301.

MCKENZIE D. P. & BICKLE M. J. 1988. The volume and composition of melt generated by extension of the lithosphere. *Journal of Petrology* **32**, 625–79.

MIDDLEMOST E. A. K. 1994. Naming materials in the magma/igneous rock system. *Earth-Science Reviews* **37**, 215–24.

MILLER C., SCHUSTER R., KLOTZLI U., FRANK W. & PURTSCHELLER F. 1999. Post-collisional potassic and ultrapotassic magmatism in SW Tibet: Geochemical and Sr–Nd–Pb–O isotopic constraints for mantle source characteristics and petrogenesis. *Journal of Petrology* **40**, 1399–424.

PATIÑO DOUCE A. E. & BEARD J. S. 1995. Dehydration-melting of biotite gneiss and quartz amphibolite from 3 to 15 kbar. *Journal of Petrology* **36**, 707–38.

PATIÑO DOUCE A. E. & BEARD J. S. 1996. Effects of P, f (O_2) and Mg/Fe ratio on dehydration melting of model metagreywackes. *Journal of Petrology* **37**, 999–1024.

PEARCE J. A. & NORRY M. R. 1979. Petrogenetic implications of Ti, Zr, Y and Nb variations in volcanic rocks. *Contributions to Mineralogy and Petrology* **69**, 33–47.

QI L., HU J. & GREGOIRE D. C. 2000. Determination of trace elements in granites by inductively coupled plasma mass spectrometry. *Talanta* **51**, 507–13.

QIU J. S., WANG D. Z., ZHOU J. C. & ZENG J. H. 1996. The geological and geochemical features of Mesozoic olivine trachyandesitic volcanic rocks in Shandong: Petrogenesis. *Earth Science–Journal of China University of Geosciences* **21**, 546–51 (in Chinese, with English abstract).

RAPP R. P. & WATSON E. B. 1995. Dehydration melting of metabasalt at 8–32 kbar: Implications for continental growth and crust–mantle recycling. *Journal of Petrology* **36**, 891–931.

ROBERTS M. P. & CLEMENS J. D. 1993. Origin of high-potassium, calc-alkaline, I-type granitoids. *Geology* **21**, 825–8.

ROGERS N. W., HAWKESWORTH C. J. & ORMEROD D. S. 1995. Late Cenozoic basaltic magmatism in the Western Great Basin, California and Nevada. *Journal of Geophysical Research* **100**, 10287–301.

ROTTURAA A., BARGOSSIA G. M., CAGGIANELIB A., DEL MOROC A., VISONAD D. & TRANNEA C. A. 1998. Origin and significance of the Permian high-K calc-alkaline magmatism in the central-eastern Southern Alps, Italy. *Lithos* **45**, 329–48.

RUDNICK R. L. & FOUNTAIN D. M. 1995. Nature and composition of the continental crust: A lower crustal perspective. *Reviews of Geophysics* **33**, 267–309.

RUPPEL C. 1995. Extensional processes in continental lithosphere. *Journal of Geophysical Research* **100**, 24187–215.

SUN S. S. & MCDONOUGH W. F. 1989. Chemical and isotopic systematics of oceanic basalts: Implication for mantle composition and processes. *In* Saunder A. D. & Norry M. J. (eds). *Magmatism in the Ocean Basins*, Geological Society of Special Publications **42**, pp. 313–45. Geological Society of London and Blackwell Scientific Publications, London.

TARNEY J. & JONES C. E. 1994. Trace element geochemistry of orogenic igneous rocks and crustal growth models. *Journal of Geological Society of London* **151**, 855–68.

TAYLOR S. R. & MCLENNAN S. M. 1985. *The Continental Crust: Its Composition and Evolution*, pp. 1–312. Blackwell Scientific Publications and Oxford Press, London.

THOMPSON A. B. & CONNOLLY A. D. 1995. Melting of the continental crust: Some thermal and petrological constraints on anatexis in continental collision zones and other tectonic settings. *Journal of Geophysical Research* **100**, 15565–79.

TURNER S., ARNAUD N., LIU J. *et al.* 1996. Post-collision, shoshonitic volcanism on the Tibetan Plateau: Implications for convective thinning of the

lithosphere and the source of oceanic basalts. *Journal of Petrology* **37**, 45–71.

WANG L. G., QIU Y. M., MCNAUGHTON N. J. *et al.* 1998. Constraints on crustal evolution and gold metallogeny in the Northwestern Jiaodong Peninsula, China, from SHRIMP U–Pb zircon studies of granitoids. *Ore Geology Reviews* **12**, 275–91.

WOLF M. B. & WYLLIE J. P. 1994. Dehydration-melting of amphibolite at 10 kbar: The effects of temperature and time. *Contributions to Mineralogy and Petrology* **115**, 369–83.

XU J., MA G., ZHU G., TONG W., GUI K. & LIU Q. 1987. Formation and evolution of the Tancheng–Lujiang wrench fault system: A major shear system to the northwest of the Pacific Ocean. *Tectonophysics* **134**, 273–310.

XU S., OKAY A. I., SENGOR A. M. C., SU W., LIU Y. & JIANG L. 1992. Diamond from Dabie Shan eclogites and its implication for tectonic setting. *Science* **256**, 80–2.

YANG J. H. & ZHOU X. H. 2001. Rb–Sr, Sm–Nd, and Pb isotope systematics of pyrite: Implications for the age and genesis of lode gold deposits. *Geology* **29**, 711–14.

YE K., YE D. N. & CONG B. L. 2000. The possible subduction of continental material to depths greater than 200 km. *Nature* **407**, 734–6.

YIN A. & NIE S. 1993. An indentation model for the North and South China collision and the development of the Tan-Lu and Honam fault systems, eastern Asia. *Tectonics* **12**, 801–13.

YU J. H., XU X. S., O'REILLY S. Y., GRIFFIN W. L. & ZHANG M. 2003. Granulite xenoliths from Cenozoic basalts in SE China provide geochemical fingerprints to distinguish lower crust terranes from the North and South China tectonic blocks. *Lithos* **67**, 77–102.

ZHAI M. G., CONG B. L., GUO J. H., LIU W. J., LI Y. G. & WANG Q. C. 2000. Sm–Nd geochronology and petrography of garnet pyroxene granulites in the northern Sulu region of China and their geotectonic implication. *Lithos* **52**, 23–33.

ZHANG H. F., SUN M., ZHOU X. H., FAN W. M., ZHAI M. G. & YIN J. F. 2002. Mesozoic lithosphere destruction beneath the North China Craton: Evidence from major-, trace-element and Sr–Nd–Pb isotope studies of Fangcheng basalts. *Contributions to Mineralogy and Petrology* **144**, 241–53.

ZHAO G., WANG D. & CAO Q. 1997. Geochemical features and petrogenesis of Laoshan granite in east Shandong Province. *Geological Journal of China Universities* **3**, 1–15 (in Chinese, with English abstract).

ZHENG Y. F., WANG Z. R., LI S. G. & ZHAO Z. F. 2002. Oxygen isotope equilibrium between eclogite minerals and its constraints on mineral Sm–Nd chronometer. *Geochimica et Cosmochimica Acta* **66**, 625–34.

ZHI X. C., CHEN D. G., ZHANG Z. Q. & WANG J. H. 1994. The neodymium and strontium isotopic compositions of Cenozoic alkali basalts from Penglai and Linqu, Shandong province. *Geological Review* **40**, 526–33 (in Chinese, with English abstract).

ZHOU T. H. & LÜ G. X. 2000. Tectonics, granitoids and Mesozoic gold deposits in East Shandong, China. *Ore Geology Reviews* **16**, 71–90.

ZHOU X. H., YANG J. H. & ZHANG L. C. 2002. Metallogenesis of superlarge gold deposits in Jiaodong region and deep processes of subcontinental lithosphere beneath North China Craton in Mesozoic. *Science in China (Series D)* **46** (supplementary), 14–25.